Author Contributions:

Conceptualization: Renée M. Fredensborg Hansen, Henriette Skourup, Eero Rinne, Knut V. Høyland
Data curation: Renée M. Fredensborg Hansen, Jack C. Landy, Ioanna Merkouriadi
Formal analysis: Renée M. Fredensborg Hansen

Arctic Freeboard and Snow Depth From Near-Coincident CryoSat-2 and ICESat-2 (CRYO2ICE) Observations: A First Examination of Winter Sea Ice During 2020–2022

Renée M. Fredensborg Hansen[1,2,3] , **Henriette Skourup[1]** , **Eero Rinne[2]**, **Knut V. Høyland[3]**, **Jack C. Landy[4]** , **Ioanna Merkouriadi[5]** , and **René Forsberg[1]**

[1]Department of Geodesy and Earth Observation, National Space Institute, DTU Space, The Technical University of Denmark (DTU), Kgs. Lyngby, Denmark, [2]Department of Arctic Geophysics, The University Centre in Svalbard (UNIS), Longyearbyen, Norway, [3]Department of Civil and Environmental Engineering, Norwegian University of Science and Technology (NTNU), Trondheim, Norway, [4]Department of Physics and Technology, UiT The Arctic University of Norway, Tromsø, Norway, [5]Finnish Meteorological Institute, Earth Observation Research, Helsinki, Finland

Abstract In the summer of 2020, ESA changed the orbit of CryoSat-2 to align periodically with NASA's ICESat-2 mission, a campaign known as CRYO2ICE, which allows for near-coincident CryoSat-2 and ICESat-2 observations in space and time over the Arctic until summer 2022, where the CRYO2ICE Antarctic campaign was initiated. This study investigates the Arctic CRYO2ICE radar and laser freeboards acquired by CryoSat-2 and ICESat-2, respectively, during the winter seasons of 2020–2022, and derives snow depths from their differences along the orbits. Along-track snow depth observations can provide high-resolution snow depth distributions which are vital for air-ice-ocean heat and momentum transfer, understanding light transmission, and snow-ice-interactions. Generally, ICESat-2 is backscattered at a surface above the elevation of the CryoSat-2 signal. CRYO2ICE snow depths are thinner than the daily model- or passive-microwave-based snow depth composites used for comparison, with differences being most pronounced in the Atlantic and Pacific Arctic. Satellite-derived and model-based snow estimates show similar seasonal accumulation over first-year ice, but CRYO2ICE has limited seasonal accumulation over multi-year ice which is linked to a slow increase in ICESat-2, and to some extent CryoSat-2, freeboards. We present a first estimation of spaceborne along-track snow depth estimates with average uncertainty of 10–11 ± 2–3 cm for 7-km segments, with random and systematic contributions of 7 and 4 cm. These observations show the potential for along-track dual-frequency observations of snow depth from the future Copernicus mission CRISTAL; but they also highlight uncertainties in radar penetration and the correlation length scales of snow topography that still require further research.

Plain Language Summary Estimates of snow depth on sea ice are currently either outdated or limited in resolution, thus a need to derive high-resolution snow depth on sea ice is crucial. Former studies have computed snow depth on sea ice using the difference in penetration between radar (Ku-band) and laser (or Ka-band radar) altimeters from different satellite missions, assuming the Ku-band radar and laser/Ka-band are reflected at the bottom and top of the snow pack, respectively. Those studies have resulted in monthly composites of snow depth due to a limited overlap of individual tracks between the satellite missions. Since the CRYO2ICE (CryoSat-2/ICESat-2 Resonance) campaign was initiated in July 2020, we have for the first time the possibility of investigating near-coincident observations of spaceborne radar and laser altimeters. These results are important to initiate relevant discussions on snow depth retrieval in preparation for the future dual-frequency altimeter mission, CRISTAL (Copernicus Polar Ice and Snow Topography Altimeter), expected to launch in 2028.

1. Introduction

In July 2020, the European Space Agency (ESA) changed the orbit of CryoSat-2 (CS2) to periodically align with National Aeronautics and Space Administration's (NASA's) Ice, Cloud and land Elevation Satellite-2 (ICESat-2, hereafter noted as IS2), a campaign named CRYO2ICE (CS2/IS2 Resonance Campaign, https://earth.esa.int/eogateway/missions/cryosat/cryo2ice, last access: 2022/03/02). With the CRYO2ICE (C2I) campaign, CS2 and IS2 now pass approximately the same location at close to the same time every 19th and 20th orbits, respectively (roughly every 31 hr, with a time difference between acquisitions of about 3 hr or less depending on the year). The C2I campaign provides, for the first time, near-coincident laser and radar altimetry at orbit-scales from space and

Funding acquisition: Henriette Skourup, Eero Rinne, Knut V. Høyland, Jack C. Landy, Ioanna Merkouriadi, René Forsberg
Investigation: Renée M. Fredensborg Hansen
Methodology: Renée M. Fredensborg Hansen, Henriette Skourup, Eero Rinne, Knut V. Høyland, Jack C. Landy
Project administration: Renée M. Fredensborg Hansen, Henriette Skourup, Eero Rinne, Knut V. Høyland, Jack C. Landy, Ioanna Merkouriadi, René Forsberg
Resources: Henriette Skourup, Eero Rinne, Knut V. Høyland
Software: Renée M. Fredensborg Hansen
Supervision: Henriette Skourup, Eero Rinne, Knut V. Høyland, René Forsberg
Validation: Renée M. Fredensborg Hansen
Visualization: Renée M. Fredensborg Hansen
Writing – original draft: Renée M. Fredensborg Hansen
Writing – review & editing: Renée M. Fredensborg Hansen, Henriette Skourup, Eero Rinne, Knut V. Høyland, Jack C. Landy, Ioanna Merkouriadi, René Forsberg

will likely advance our understanding of how different snow and sea ice properties may impact the signals received by satellite radar and laser altimeters.

An important parameter governing the growth and melt of sea ice is snow, due to its insulating and reflective properties. The depth of snow on sea ice varies on short spatial and temporal scales depending on weather patterns and surface conditions (Liston et al., 2018; Moon et al., 2019). Snow depth on sea ice has been estimated from spaceborne sensors using passive microwave observations (Markus & Cavalieri, 1998). However, these observations have relatively coarse resolution (12.5 km or more) and have either been primarily obtained over first-year ice (FYI) (Markus & Cavalieri, 1998), allowed for multi-year ice (MYI) coverage though limited to the spring due to calibration with airborne reference observations (Rostosky et al., 2018; Zhou et al., 2021), or have simply not been provided as publicly operational, daily products. Snow depth on sea ice has also been estimated utilizing the difference in penetration between spaceborne altimeters at different frequencies (e.g., Garnier et al., 2021; Guerreiro et al., 2016; Kwok et al., 2020; Lawrence et al., 2018). Monthly gridded estimates have been published using either laser and Ku-band (LaKu) altimeter observations (Kacimi & Kwok, 2020, 2022; Kwok et al., 2020) or Ka- and Ku-band (KaKu) altimeter observations (Garnier et al., 2021; Guerreiro et al., 2016; Lawrence et al., 2018) in both hemispheres. This is done by assuming that laser/Ka-band signals backscatter at or close to the air-snow interface (Garnier et al., 2021; Guerreiro et al., 2016) and that the Ku-band signals fully penetrate the snow pack, or by calibrating Ka-band and Ku-band freeboards to the air-snow and snow-ice interfaces, respectively, using airborne observations available from the western Arctic (Lawrence et al., 2018). However, recent studies suggest that complete and zero backscattering horizons assumed for Ku- and Ka-band frequencies, respectively, are not necessarily valid for all conditions of the Arctic snow and sea ice pack (King et al., 2018; Nab et al., 2023; Nandan et al., 2023). Furthermore, the roughness within the footprint of the satellite at the scale of sea ice features (like ridges or leads) or small-scale roughness at the scale of the signal wavelength also impact the height of the mean backscattering intensity (Landy et al., 2020). Dual-frequency altimeter techniques generally observe Arctic snow depths of about 0.10–0.15 m at the beginning of the winter season increasing to about 0.20–0.25 m by the end of the winter (Kacimi & Kwok, 2022). However, the methods typically filter or average the altimeter height differences over long spatial and temporal intervals. Thus, they do not resolve the local space-time variability of the snow depth nor the covariability between altimeter signals.

With the upcoming launch of ESA's CRISTAL (Copernicus Polar Ice and Snow Topography Altimeter) mission expected in 2028, it is important to investigate the potential of snow depth retrieval along the satellite orbit. CRISTAL will carry a dual-frequency (KaKu) altimeter for the purpose of retrieving snow depth variability along track. One of the mission requirements of CRISTAL is to provide sea ice freeboard (height of sea ice above local sea level) with an accuracy of 0.03 m along orbit segments of less than or equal to 25 km, and deliver sea ice thickness measurements with a vertical uncertainty of less than 0.15 m along the same orbit segments (Kern et al., 2020). To achieve this, snow depths need to be obtained along the same orbit segments with an uncertainty of less than or equal to 0.05 m (Kern et al., 2020). This calls for an urgent investigation of altimeter-derived snow depth along orbit-segments of 25 km or less, which the C2I campaign provides the first-ever opportunity to investigate, with the caveat that CRISTAL carries a Ka-band radar instead of the green laser of IS2. High spatial and temporal resolution observations from C2I can be used to examine the assumption of full CS2 signal penetration when compared with reference observations, which is crucial since uncertainties on the snow load and signal penetration constitute the largest sources of systematic error in sea ice thickness estimates derived from altimetry (Landy et al., 2020). Providing such high-resolution observations of snow depths will likely reduce the uncertainty in sea ice thickness observations from altimeters, since they currently require an estimate of snow mass loading to compute sea ice thickness.

The aim of this study is to make a first examination of the feasibility of obtaining along-track snow depth observations over sea ice using the difference between laser and radar freeboards from near-coincident spaceborne observations. The study discusses steps for making observations of different resolution comparable over sea ice and present first results of snow depth from C2I. These observations are compared with auxiliary snow depth data derived from passive-microwave observations, reanalysis-based models, and in-situ observations. Furthermore, aspects that may impact the derived freeboard are discussed in relation to the derived snow depth estimates. This study provides insight into the comparison of altimeter data over sea ice with different footprint scales, for capacity building before the launch of CRISTAL. We note, that the laser observations of IS2 and the Ka-band radar to be mounted on CRISTAL will not sample the target surface in the same manner, thus a C2I analysis shall not be considered as a CRISTAL simulator. However, the first-ever near-coincident spaceborne LaKu observations

provide the opportunity to focus on the advantages and challenges of dual-frequency altimetry for snow depth estimation along orbit scales, particularly regarding issues of footprint size and Ku-band radar penetration. A discussion of the differences between laser and Ka-band altimetry, and implications of these differences for results presented herein is also provided.

2. Data and Methods

We investigate C2I observations from the two available winter seasons (November–April 2020–2022). By investigating entire winter seasons, we expect several processes to have occurred within the snow- and ice pack (e.g., snow grain metamorphism, flooding, refreezing, differences in snow depth due to accumulation of snow throughout the season, deformation of ice resulting in increased surface roughness, melting, freeze-up, measurements of thinner ice or thicker ice), all affecting the snow pack on the ice and potentially the mechanisms by which the altimeter radar and laser signals interact with the snow.

2.1. IS2 Data

IS2 is a photon-counting laser altimeter which transmits laser pulses split into a six-beam configuration of three beam pairs (each having a strong, GTR, and weak beam, GTL) (Neumann et al., 2019). With a 10 kHz pulse-repetition-frequency, it leads to a 0.7 m along-track separation and allows for an unprecedentedly dense surface-sampling at footprints of about 11 m at nominal altitude (Magruder et al., 2020). From these photons, surface segments are derived by aggregating 150 photons, and based on a radiometric classification, segments from leads and floes are identified and produced in the ATL07 product (Sea Ice Heights). Along-track freeboards are calculated in the ATL10 product based on a reference sea surface derived from the available lead/sea surface segment heights, resulting in inconsistent segment-lengths depending on surface reflectivity and specularity. A single reference sea surface estimate is produced for consecutive 10 km along-track sections that include at least one sea surface sample, for each beam independently. Negative freeboards are set to zero (Kwok et al., 2020; Petty et al., 2021). IS2 observations are unavailable in the presence of clouds (Fredensborg Hansen et al., 2021), and cloud-impacted photons are removed during processing which results in gaps along the track (e.g., Figure 1). ATL07 recently refined the surface finding procedure (the identification of leads for sea surface height segments), where surface classifications such as dark leads have been removed (keeping only specular returns as leads) which has improved the performance (Kwok et al., 2021). A recent study (Ricker et al., 2023) suggested that weak beams, with ∼1/4 of the photon rate compared to strong beams, can provide useful information along the track and should be considered even if this is not what the operational monthly freeboard product (ATL20) currently does (Kwok et al., 2022). Based on these findings and due to the limited coverage of C2I observations, we shall include all six beams when binning the data to comparable resolutions (see Section 2.5). For this study, we make use of release 005 (r005) ATL10 observations, even though the latest release is r006. This is due to the C2I identification tool (www.cs2eo.org, last access: 2024/01/22) currently not having included the latest release. In addition, we utilize ATL20 (Monthly Gridded Sea Ice Freeboard, v004, see Petty et al. (2020)) to create, in combination with gridded CS2 radar observations, monthly composites of LaKu snow depth products for comparison purposes.

2.2. CS2 Data

CS2 data has a larger footprint (∼300 m × 1,650 m, see e.g., European Space Agency, 2019; Scagliola, 2013, in synthetic aperture radar (SAR) mode and samples at a rate of 20 Hz approximately every 300 m) than IS2, thus it will be used as the reference resolution for the C2I observation to ensure as consistent spatial resolution as possible when comparing sensors. To examine the sensitivity of the freeboard and snow depth to different re-trackers (a processing estimation approach used to determine the range to the ground target) and/or processing methods, we have included three different products when possible: two using empirical re-trackers, and one using a physical re-tracker.

- *Baseline-E Ice radar freeboard (ESA-E)*: We use data acquired by the SIRAL Ku-band interferometric SAR altimeter mounted on CS2 in SAR mode, the primary mode over sea ice. We make use of the Level 2 (L2) Ice product processed at the Baseline-E version. We extract the radar freeboard, which has been derived using combined waveform re-trackers: (a) for diffuse waveforms, expected to originate from ice floes, a 70% threshold-of-first-peak re-tracker, and (b) for specular echoes, expected to originate from leads, a peak-finder based on the model-fitting method described in Giles et al. (2007). CS2 ESA-E data have been pre-processed
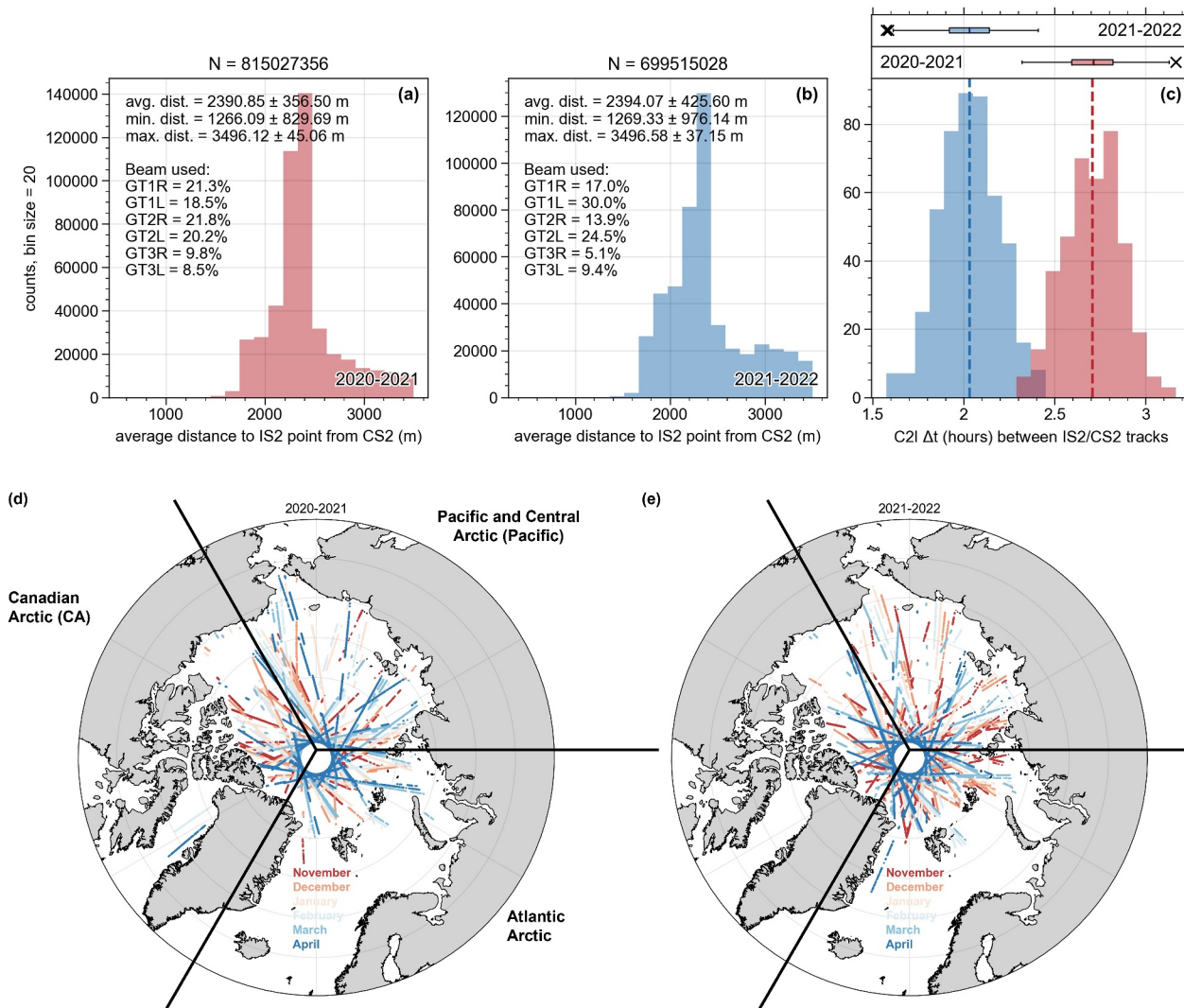
Figure 1. (a–b) Distance between CryoSat-2 (CS2) and the ICESat-2 (IS2) observations used to generate the CRYO2ICE (C2I) samples for winter seasons 2020–2022, (c) time-lag between CS2 and IS2 (per C2I) tracks for both winter seasons, and (d–e) locations of all used C2I tracks for both winter seasons along with the separation into geographical areas used in the analysis later.

to remove erroneous points using the error flags available in the L2 product following the procedure described in Text S1 in Supporting Information S1.

- *Lognormal Altimeter Re-tracker Model (LARM) radar freeboard*: Landy et al. (2020) presented a physical re-tracker which varies the percentage threshold that is being re-tracked according to the large-scale roughness of the sea ice, based on model simulations of the radar altimeter echo assuming a log-normal distribution of the surface roughness (Landy et al., 2019). The same re-tracker is also automatically applied to leads, which have negligible roughness and therefore a re-tracking threshold >98%.

- *Climate Change Initiative+ (CCI+) radar freeboard*: Another commonly used CS2 product is the CCI+ Climate Record Data Product (CRDP), which also employs the empirical first-threshold-of-peak re-tracker, however with a percentage threshold of 50% for both sea ice floes and leads. At the time of writing, the CCI+ product is only available until end of winter season 2020–2021.

It may be the case that for some ESA-E observations there are no CCI+ or LARM observations available, or vice versa, due to different filtering schemes applied by the providers. However, when comparing statistically, we shall only compare observations where there is coverage by all three re-trackers unless otherwise noted. The pre-processing steps and steps to identify corresponding observations between different data sets are discussed in Text

S1 in Supporting Information S1. CCI+ and LARM are also available as monthly gridded products, which are used in combination with the respective ATL20 products to generate LaKu composites for comparison.

2.3. Independent Data

A comparison between the derived C2I snow depth and independent snow depth estimates is necessary to evaluate the performance of the algorithm. Due to limited coverage by C2I and lack of dedicated reference campaign observations, we have limited in situ observations to compare with. Instead, we will primarily compare C2I-derived snow depth with snow depth estimates computed from passive microwave observations over FYI and reanalysis-based numerical snow evolution schemes for all sea ice types. This comparison is not meant as a validation, since we cannot be sure that any of these products represent the truth. However, the comparison provides a means of evaluating the snow depths derived from altimetry against the state-of-the-art snow products currently used for scientific applications including estimating sea ice thickness. For each available C2I snow depth observation, the nearest gridded point from the basin-scale estimates are extracted and used for comparison. The following snow depth products are used:

- *Advanced Microwave Scanning Radiometer (AMSR2)*: we make use of the daily snow depth product computed from a 5-day average (Meier et al., 2018), following the methodology of Markus and Cavalieri (1998). The product excludes the Arctic perennial ice regions due to microwave volume scattering making retrieval of snow depth on MYI ambiguous and snow depth estimates over MYI are therefore not available. The snow depth retrieval methodology of AMSR2 is applicable only to dry snow (Markus et al., 2017). We further extract the sea ice concentration parameter computed using the method described by Markus and Cavalieri (2000), Markus and Cavalieri (2009). Both snow depth and sea ice concentration are provided on a swath-level basis and afterward averaged out to daily estimates (from 5-day aggregates) on a 12.5 km polar stereographic grid.
- *SnowModel-LG (SMLG)*: SMLG is a snow evolution modeling system that produces daily snow depth and density distributions over Arctic sea ice from 1 August 1980, and onward. SMLG resolves physical snow processes such as sublimation from static surfaces and blowing snow, snow melt, snow density evolution, snow temperature profiles, energy and mass transfers within the snow pack, and superimposed ice (Liston et al., 2020).
- Warren et al. (1999) *(W99) and modified W99 (mW99)*: W99 presents a pan-Arctic monthly (October–April) climatology of snow depth estimates derived from reference observations carried out during the 1950–1990s (Warren et al., 1999). Kurtz and Farrell (2011) showed, through a comparison with airborne observations, that mW99 overestimates snow depth estimates of FYI by about a factor of 0.5 for more recent years. Thus, it is common practice for altimetry studies using mW99 to apply this correction factor. ESA-E provides mW99 estimates per CS2 observation, which we include in the analysis. In addition, mW99 gridded products are used to provide an additional comparison with monthly LaKu composites.

2.4. Identification of Relevant C2I Data

Utilizing the publicly available C2I tool (www.cryo2ice.org, last access: 2022/03/02; now updated to www.cs2eo.org) developed by EarthWave (Alford et al., 2021), we identified relevant C2I orbits for the period of November to April for 2020–2022. We retrieved monthly C2I tracks provided the CS2 and IS2 orbits were within a 10 km separation distance, had less than 4 hr between the respective acquisition times and that the intersection time of the orbits was more than 1 min. Using these criteria and application of the full pre-processing and data binning methodology (Section 2.5) resulted in a total of 358 and 415 C2I tracks for 2020–2021 and 2021–2022, respectively, relatively evenly spaced in time and geography, over the winter season under investigation (Figures 1d and 1e). Here, we see that on average a temporal lag between C2I tracks of 2.71 hr in 2020–2021 and 2.03 hr in 2021–2022, see Figure 1c. It is also worth noting, that while more tracks were available for 2021–2022, fewer C2I samples where available along the tracks (815,027,356 for 2020–2021 vs. 699,515,028 for 2021–2022, Figures 1a and 1b).

2.5. Data Binning of C2I Data

The aim is to obtain the highest possible spatial resolution of the estimated snow depth that is, close to the sampling interval of CS2, however the real challenge is ensuring that the CS2 and IS2 observations are

statistically comparable after binning. We are likely to require a radius for binning the observations that is larger than the radius of the theoretical CS2 pulse-limited footprint (∼850 m, as was used in Bagnardi et al. (2021)), since observations from the two sensors are rarely coinciding at this radius (not shown). Since IS2 observations closest to the CS2 observation should be more representative of the surface observed by CS2, we assign a higher priority to these observations. Therefore, the downsampled IS2 freeboard observations are derived with linear inverse distancing weights applied. However, it is still important to consider how large a search radius, centered at each CS2 nadir point, to be used when binning IS2 to the same location as CS2. The choice of search radius is a compromise between the spatial coverage (along-track number and density of snow observations along C2I track) and representation of the surface. The analysis presented in Figure S1 and Text S2 in Supporting Information S1 shows the variance of the freeboard differences between CS2 and IS2 as a function of the along-track binning radius. It is evident from Figure S1 in Supporting Information S1 that the variance, which is computed from C2I tracks in November/December 2020, is higher for a search radius equal to the CS2 pulse-limited footprint (∼850 m) than for higher search radii and that the variance decreases to a saturation point around 2,000 m. We note, that this analysis is not a semivariogram, as we are not interested in identifying at which lengths and time-lags the data points are no longer correlated. Instead, we aim to find a search radius along the C2I orbits, that allows for inclusion of enough data without smoothing too much signal. We conclude that a search radius of 3,500 m provides comparable results to the case where we use a lower search radii (saturation point around 2,000 m), but significantly increases the number of observations. The distance of the IS2 samples to the nadir point of CS2 is, on average, 2,390 ± 357 m (2,394 ± 426) for 2020–2021 (2021–2022, see Figures 1a and 1b), using a maximum radius of 3,500 m to include all six beams in an ideal coincidence scenario). The radar observations contain speckle noise (i.e., not fully depressed by multi-looking) and shot-to-shot-variability based on surface conditions within the footprint, and as such, the freeboard observations at the nominal 20 Hz CS2 sampling rate are expected to be noisier than the true ice elevation variability. To make the IS2 and CS2 observations comparable, we therefore smooth the CS2 freeboards with a 3,500 m radius as well (∼7 km moving average window), limiting the impact of speckle and other sources of random noise in the process. When generating orbit-based segments of 25 km, we separate the along-track distance into segments of 25 km and appoint the observations to the nearest segment point using the haversine formula, thereafter the segments are averaged.

2.6. Considerations Regarding Sea Ice Drift During C2I Time-Lag

Sea ice is in constant motion, drifting along with the wind and currents. Ideally, the C2I observations would be drift-corrected since there are several hours between acquisitions (between ∼1.5–3 hr, see Figure 1). However, with limited sea ice drift observations available with pan-Arctic coverage (to ensure coincidence with all C2I tracks), and at high temporal resolution (ideally hourly, but at maximum 24 hr time-lag) and spatial resolution (25 km or less), we need to further evaluate whether the C2I will move significantly (>3.5 km or even further) as it will move the ice out of the search area and smoothing window applied to the C2I observations. To evaluate this, we use the Medium Resolution OSI SAF sea ice drift product (EUMETSAT, 2024) derived from visible and infrared observations, which provides 24-hr displacement products four times a day (every 6 hr) at a grid-resolution of 20 km. Due to the observations being in the visible/infrared spectrum, there is a potential for data not being available (for winter season 2020–2021, 17.51% of the drift-estimates were not-a-number). For each C2I track, the closest OSI SAF drift product is identified and used to extract the v- and u-displacement variables, which are then delineated using 24 hr assuming constant drift to provide an hourly estimate. For each C2I observation, the nearest-neighboring OSI SAF drift (u- and v-displacements) is extracted along with the uncertainty (equal for both displacements). From the displacements, we compute sea ice drift (z) using $z = \sqrt{(v^2 + u^2)}$. We investigate only the winter season of 2020–2021 due to issues with the drift product after that season, which at the time of writing OSI SAF was trying to resolve.

Here, we observe an average drift of 2 km during winter season 2020–2021 for the C2I samples (see Figures 2a–2c). Only 14.14% of the data available drifted more than 3.5 km during all C2I observations in winter 2020–2021. Median absolute u- and v-displacement was 1.02 km/C2I time-lag and 0.96 km/C2I time-lag, respectively, showing that the C2I samples at ∼2 hr time lag typically have ice drift significantly lower than half of the 7-km averaging window. We also estimated relative uncertainties for drift, v- and u-displacement, since we work with fractions of the original product (see Figures 2d–2f), where relative uncertainties are computed using $U(\%) = U/x$, with U denoting the uncertainty of drift, or each displacement, and x denoting the observation. The uncertainty of
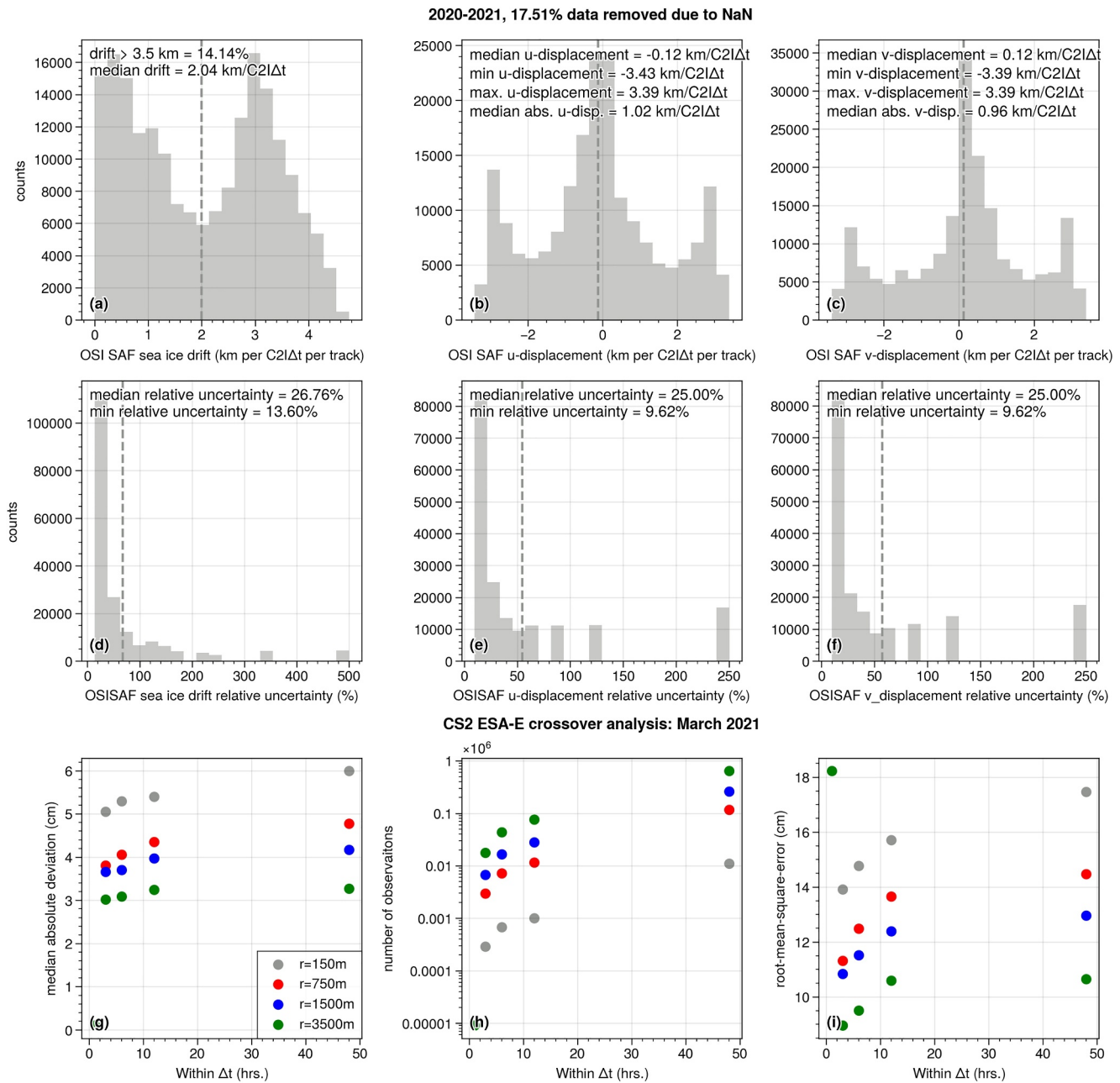
Figure 2. (a–c) estimated drift, *u*- and *v*-displacement for nearest-neighboring OSI SAF medium resolution drift observations for each C2I observations during winter 2020–2021. (d–e) derived relative uncertainties for (a–c). (g–i) crossover (XO) analysis of all CS2 ESA-E tracks on March 2021 to estimate how large an impact potential drift might have on the freeboards.

the sea ice drift is computed assuming dependency (as it is given by the same value), which equals $U(z) = U(v) + U(u)$. The relative uncertainties range from a minimum of 9.62% for displacements or 13.60% for drift, with median relative uncertainties ∼25%–26%. According to Taylor (1997), relative uncertainties of 10% or beyond suggest that the variable represents a crude estimate.

To estimate how big an impact drift appears to have on the freeboards, we computed a CS2 ESA-E cross-over (XO) analysis for various time-lags and search distances for March 2021, see Figures 2g–2i. Here, we use median-absolute-deviation (MAD) and root-mean-square-error (RMSE) as estimates of precision. MAD and RMSE both increase as a function of the averaging radius and time-lag. The number of observations also declines rapidly when imposing stricter limits on the radius and time lag. The decrease in precision with time lag shows that the

two sensors are more likely to be observing the same ice at 3 hr compared to 6 or 12 hr. But the difference in statistics is relatively small, so the uncertainty stats calculated for 3 hr lag are likely to be a good approximation for the uncertainties at 0 hr lag. Figures 2g–2i shows one instance where XOs were identified with time-lag less than 1 hr, and here MAD is significantly lower (0.15 cm) and RMSE is the highest for all the analyses. This is caused by the search radius applied (3,500 m), where it likely identified XOs between two tracks, even though those tracks are likely the same but the orbit number has changed when crossing the Arctic, prompting the algorithm to search the next file for a XO in the successive orbit file. With the search radius being large enough to overlap with a successive orbit, this may explain why observations are so similar, and the change in time is negligible.

2.7. Snow Depth From Differences in Laser and Radar Altimetry

Following Kwok et al. (2020), we calculate the snow depth by differencing laser and radar freeboards. Assuming a simple-layer geometry of sea ice floes, one can express snow depth (h_s) as the difference between the total freeboard (h_f), as measured by IS2, and the sea ice freeboard (h_{fi}):

$$h_s = h_f^{IS2} - h_{fi}. \tag{1}$$

The sea ice freeboard (h_{fi}) is related to the radar freeboard measured by CS2 (h_{fi}^{CS2}) following:

$$h_i = h_{fi}^{CS2} + h_s(\eta_s - 1). \tag{2}$$

Here, η_s is the refractive index at Ku-band, $\eta_s = c/c_s \cdot (\rho_s) = (1 + 0.51\rho_s)^{1.5}$ (Ulaby et al., 1986), and c is the speed of light in free space. The second term in Equation 2 accounts for the reduced propagation speed of the radar wave (c_s) as it travels through the snow pack with a bulk density ρ_s. It is assumed, that at temperatures below freezing, at the wavelengths of IS2 and CS2, that the laser and radar returns come from the air-snow and the snow-ice interfaces, respectively, resulting in observations of total and sea ice freeboards (when accounted for delay in pulse propagation through snow). The validity of this assumption has been discussed in several studies (King et al., 2018; Nandan et al., 2017; Tonboe et al., 2021), and implications thereof are discussed in Section 3.1. Through combination of Equations 1 and 2 and solving for h_{fs}, snow depth is given by:

$$h_s = \frac{\left(h_f^{IS2} - h_{fi}^{CS2}\right)}{\eta_s} \tag{3}$$

Now, snow depth (h_s) is related to the differences between the IS2 and CS2 freeboard (the observables) with one free parameter, η_s, which is dependent on the bulk snow density. For this study, we shall keep the bulk density of snow constant at 300 kg·m^{-3}, producing $\eta_s = 1.24$, and discuss the impact of this assumption further in Section 3. The equations defined here also follow the definitions of Garnier et al. (2021). We note, that negative snow depths are not removed from the analysis and they currently make up less than 3% of the data for both seasons and with a negligible impact (not shown). However, assuming errors of ∼8 cm from XO analysis in Figure 2i, a single observation over thin snow could have a negative snow depth owing to the error. Thus, removing negative snow depths would result in overlooking the impact of the random error. We cannot remove the negative depths without removing positive depths with a high error, but we do not know which samples have a high error, so it is most fair to retain all the observations.

In addition to investigating observations and derived snow depth along C2I orbits, we also compute monthly LaKu snow depth composites from IS2/CS2 (LARM or CCI+). The LaKu estimates are computed from available gridded CS2 LARM/CCI+ radar freeboards and IS2 ATL20, which has been re-gridded to a common 50 km EASE2 grid using the nearest-neighbor. To account for slower propagation speed through the snow pack, a constant snow density of 300 kg/m^3 is assumed. These products are used to compare the C2I distributions and accumulation rates across the seasons to identify limitations and differences between gridded and along-track estimates.

The snow depth estimates along C2I orbits are also compared with in situ observations from either acoustic snow depth buoys from the Alfred Wegener Insitute (AWI) or seasonal ice mass balance buoys (SIMBA) measuring with thermistor stirngs. In total, four acoustic buoys and two thermistor string buoys are used in the evaluation of the derived snow depths (see Text S3 in Supporting Information S1). When comparing with reference observations, the buoy observations are first post-processed to daily snow depth estimates at the average daily location. We identify comparable C2I points assuming they are within ±50 km and 2 days of the buoy locations and acquisition time following Ricker et al. (2015).

2.8. Uncertainty Calculation of C2I Snow Depths Combining Random Errors and Systematic Biases

To compute the precision (or an estimation of random errors) of freeboard and snow depth observations, a XO analysis of the C2I tracks (at C2I resolution of 7 km) across the full winter-season is conducted. For each C2I track, each file is compared with all subsequent C2I tracks of that season. If the difference in time (Δt) between files is less than the required time-lag (e.g., 24 hr, 6 hr, or more), that specific track is saved for further analysis. Each observation of the original file, used as baseline, is compared with all the observation points extracted from files within Δt. All points within a search radius of 3.5 km are used, and an average value –per baseline observation –from both the baseline product and all points within Δt are computed, yielding XO points for the three CS2 re-tracked radar freeboards and the IS2 total freeboards. For all XOs across one season (due to the limited C2I observation points), we compute one estimate of precision by root-mean-square-deviation (RMSD), which we assume to represent a minimum estimate of the random error contributions for each freeboard contribution. The random errors in radar freeboard could have multiple sources that are challenging to isolate. For instance, radar speckle, coming from strong reflections of sea ice surfaces oriented perpendicular to the antenna bore-sight, could bias the retrieved elevation high or low. Random "snagging" of the radar return to level ice areas around the nadir point of the footprint could lead to artificial elevation variability. Radar scattering from reflective layers in the snow pack and any deviation of the footprint-scale surface topography away from the assumed distribution of the retracker (i.e., Gaussian for ESA-E, Lognormal for LARM) could also lead to random elevation errors from the retracking algorithm. The random error contribution of the C2I uncertainty is then computed from the precision estimates of CS2 and IS2 freeboards, assuming they are independent. Random errors are only part of the overall uncertainty, as we must also consider the possibility for systematic biases. Since we are working with three different freeboard-retrieval-methodologies, we make a first attempt to estimate systematic bias from the retrieval methodology, by estimating the bias (or difference) between freeboards. As such, per C2I point we estimate the freeboard difference between the three re-trackers and use the maximum absolute height difference between re-trackers per C2I point as a measure of systematic biases. There are other sources of systematic bias beyond the retracking bias, such as potential under-penetration of the Ku-band radar into the snow pack. However, these other sources are challenging to estimate on an along-track basis and may be compensated by the retracking bias. We take the retracking bias as a first approximation for the systematic uncertainty. To compute overall uncertainty, we assume at these length scales (C2I resolution at ~7 km using the 3.5 km search radius) that the random and systematic errors are independent. Thus, we can estimate a measure of uncertainty ($U(C2I)$) using $\sqrt{U(R)^2 + U(S)^2}$, where $U(R)$ and $U(S)$ are the uncertainties of the random errors and systematic biases, respectively (Taylor, 1939). There are fewer CCI+ observations available than LARM and ESA-E in the XO analysis. To keep as many observations as possible, we keep them all and note that for observations where CCI+ and/or LARM are not available, fewer inputs are available for the systematic bias estimation in that observation location. For 2020–2021, there were 429 CCI+ XOs with a maximum time-lag of 24 hr, whereas there were 2,634 LARM and 2,817 ESA-E. For 2021–2022, there were 2,398 ESA-E and 2,391 LARM observations, and no CCI+ observations were available for that entire season.

3. Results, Discussion and Conclusions

3.1. Freeboards and Associated Snow Depths Along-Track

The freeboards of CS2 and IS2 binned to a similar resolution (C2I) are shown for one pair of tracks in November, January, and March in Figures 3a, 3c, and 3b, 3d–3f, respectively. The tracks are ~500–600 km long. Here, it generally shows that IS2 has higher freeboards than CS2, as expected based on the assumption that IS2 pulses are reflected at the air-snow interface (typically the first surface encountered). However, it can be seen several times how individual CS2 20 Hz observations exceed the freeboards observed by IS2. This could be due to: (a) the
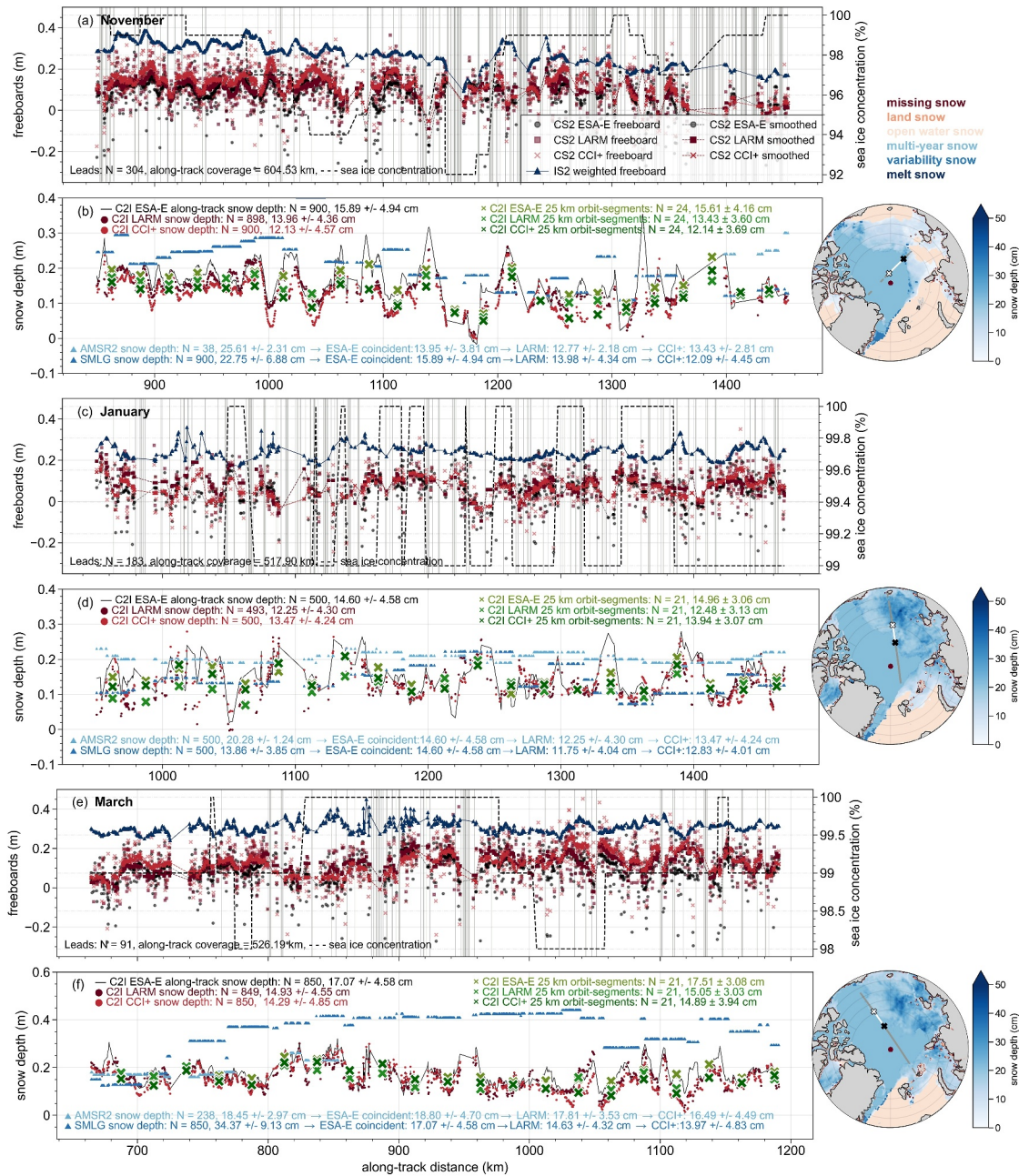
Figure 3. Subset of C2I track with (a) CS2 Baseline-E (ESA-E), Lognormal Re-tracker Altimeter Model (LARM) and Climate Change Initiative (CCI+) radar freeboard, IS2 weighted laser freeboard and associated AMSR2 sea ice concentration for 10 November 2020. CS2 ESA-E identified leads are shown in vertical gray lines, number of leads in the subset is denoted on the subplot along with the along-track coverage of the subset; (b) C2I along-track snow depth using different re-trackers and associated snow depth from AMSR2 and SMLG for 10 November 2020. C2I snow depths at 25 km orbit segments (one value pr. segment) are provided as well. The pan-Arctic map showing AMSR2 snow depth estimates and classifications (open water, multi-year ice etc., presented by the legend above the first map) also shows the location of the track and subset; gray denote the entirety of the track, white is the subset of the C2I track, white cross denotes the beginning and black cross the end of the subset; (c–d) same as panels (a–b) for C2I track on 30 January 2021; (e–f) same as panels (a–b) for C2I track on 17 March 2021.

binning methodology, where more of the used IS2 points originate from level/thinner ice whereas the paired CS2 point is sensitive to thicker ice or an area of rougher surface topography; (b) noise/speckle in the CS2 data; (c) noise in the IS2 data; (d) shot-to-shot variability in CS2 caused by surface conditions within the CS2 footprint that are not reflected in the IS2 observations or vice versa; and/or (e) sea ice drift occurring between tracks which have not been possible to account for. Significantly more leads are observed in the track from November than in January or March. This is expected, due to the thinner and less dense ice cover in November compared to a

consolidated ice cover at the end of the winter in March. However, the presence of leads can also impact the derived freeboard. In areas where there is more open water and leads, the waveforms are more likely to experience off-nadir reflections within the footprint and waveform snagging (Armitage & Davidson, 2014), which will bias the CS2 radar freeboard high. However, in most cases, these snagged waveforms will be removed by the quality flag in the pre-processing or flagged as "ambiguous" in the waveform classification routine and discarded. Furthermore, having a limited number of lead observations will impact the interpolated instantaneous sea surface height anomalies observed from the leads, and as a consequence impact the derived freeboard. As an example, we see a sudden decrease in sea ice concentration in November around 1,150 km along-track, which coincides with raw CS2 freeboards being higher than IS2 total freeboards. This combination will result in negative snow depths, where the high CS2 freeboards could be caused by the presence of open water and a potential increased presence of leads within the footprint of CS2 which can cause snagging of the waveforms resulting in anomalously large freeboards.

From these freeboards, we can derive snow depths following Equation 1, which are shown in Figures 3b, 3d, and 3f. The C2I CS2 freeboards at raw sampling rate show higher along-track variability which will result in higher snow depth variability when compared to the SMLG simulations and AMSR2 observations available at 12.5–25 km resolution. Through the comparisons of observations from three different re-trackers, we investigate differences in snow depth depending on the selection of re-tracker. It is noteworthy that the re-trackers are most consistent over the track from January covering only FYI, which may suggest the freeboard is most sensitive to the re-tracking step over MYI. Due to the complexity of a snow pack on MYI (where processes such as re-freezing, snow-ice formation, ice lens formation, could have occurred) it is likely that the radar scattering horizon might occur somewhere within the snow pack rather than at specific clearly defined interfaces (such as snow-ice or air-snow). This effect might be causing the discrepancies observed in the March track (late season). Surface roughness (large scale, >0.5 m) such as ridges within the footprint may also impact the scattering horizon and backscattered signal, causing the re-tracked surface elevation to be shifted low toward level ice areas of the radar footprint.

While the basin-scale snow depth estimates are from gridded products and of coarser resolution with less variability, it still provides an interesting comparison. For the track in January, we have a significant number of comparable observations, and on average along the track AMSR2 appears to observe consistently thicker (+0.05 m average with more than 10 cm for the November track) snow than C2I, which may be due to CS2 not penetrating through to the snow-ice interface, AMSR2 overestimating the snow depth or might be caused by spatial and/or processing differences between the products. In comparison, the track of March has some points to compare ($N = 238$) for AMSR2 and here, the AMSR2 observations are much closer (on average within 1 cm) to the C2I observations, whereas the SMLG simulations vary significantly from C2I. In the comparison with SMLG, simulations are available for FYI and MYI and thus, a more comprehensive evaluation can be done. Here, higher similarity is observed between the tracks of January when comparing with average observations (0.02–0.04 m of difference), whereas SMLG features thicker snow in November (>0.07 m difference on average). SMLG also features more variability than AMSR2 snow depths, and has a more consistent variability to the C2I observations. Here we note that AMSR2 is a 5-day averaged product used to create a daily composite, which may reflect the limited variability observed. Sea ice can easily drift through a couple of the AMSR2 grid cells over the 5-day window which has the effect of diminishing the actual spatial resolution such that the grid on which the data is supplied is not indicative of the real resolution. Furthermore, should there be a C2I overpass before a snowfall event, the AMSR2 5-day window will feature that snowfall in the daily composite and be biased high on the day of the C2I overpass. Large differences are observed in the track from March, with SMLG simulating 0.10–0.15 m thicker snow than the C2I observations. For SMLG this likely identifies new snow accumulation that has occurred during the season, and is thicker than C2I which has a snow depth similar to January albeit for a different location. This highlights the possibility that CS2 does not fully penetrate the snow pack over MYI. As an example, SMLG consistently features high snow depth with little variability between 800 and 1,000 km along-track in March, whereas C2I shows high variability with overall lower snow depths for the same location (Figure 3f). It should be noted that SMLG does not account for snow loss due to snow and sea ice interactions, potentially overestimating snow depth over level, undeformed ice. SMLG was recently coupled with a 1D thermodynamic sea ice model (HIGHTSI; Launiainen & Cheng, 1998), to investigate snow losses in processes such as snow-ice formation, that is, ice that forms at the sea ice surface as a result of flooding at the snow/ice interface due to negative freeboard conditions (e.g., Leppäranta, 1983), and sea ice dynamic processes, that is, the preference of snow to accumulate

on the lee side of sea ice roughness elements such as ridges and ice deformations. Snow and sea ice interactions should result in the reduction of snow depth over level sea ice, with potential of the bottom snow layers being incorporated into the sea ice over level ice areas (Merkouriadi et al., 2020), and largely uneven distribution of snow depth between level and deformed ice (Itkin et al., 2023).

3.2. Variations of Coincident C2I Snow Depths Across the Winter Season 2020–2022

We investigate two winter seasons of observations to evaluate how well the C2I observations compare with dual-altimetry observations at pan-Arctic monthly scales. Here, we present bi-monthly distributions of C2I snow depths (Figures 4 and 5) from 25-km segments separated into three study regions (Figure 4, areas defined in Figures 1d and 1e). We note from the pan-Arctic (C2I) maps that relatively thicker snow is present over the Canadian Arctic (CA) and thinner snow over the marginal seas (Pacific and Central Arctic (PA), and Atlantic Arctic (AT)), see Figures 4m–4r and Figures 5j–5l. For 2020–2021, C2I snow depths in CA reach approximately 0.21 ± 0.07 m (one standard deviation) by the end of the accumulation season, whereas SMLG features slightly thicker snow depths with identical standard deviation of approximately 0.25 ± 0.07 m. The largest discrepancies between the model and C2I observations occur in the AT and PA regions, where C2I observes lower snow depths with a narrower distribution. This is correlated with the storm tracks and precipitation events that act to enhance snow depth in the model, especially later in the accumulation season, that is not represented in the satellite observations (Zhou et al., 2021). The satellites generally observe thicker snow in CA which reduces gradually to thinner snow across the Atlantic and Pacific sectors (Garnier et al., 2021; Guerreiro et al., 2016; Kacimi & Kwok, 2020; Lawrence et al., 2018). It is worth noting that the acoustic snow buoys (Text S3–S7, Figures S2–S5, and Table S1 in Supporting Information S1) observed clear snow accumulation events in spring 2021, whereas spring accumulation was low or absent in the SIMBA observations (Figure S4 in Supporting Information S1), which suggests that both the satellite observations could be missing information or the models may overestimate, but also that the comparison with local-scale buoy estimates can prove challenging. Comparison with acoustic and thermistor string buoys (at original C2I resolution) shows inconsistent results regarding snow accumulation and conclusions are difficult to derive. Correlations are weak when compared to acoustic buoys, where significant accumulation is observed (up to ∼70 cm snow depth by February for some buoys), which is not reflected by either C2I nor SMLG, nor by the thermistor string buoys (see Figure S4 in Supporting Information S1). Here, on level ice, the thermistor string buoys observes snow depths up to 25–30 cm by beginning to end of Spring similarly to C2I, with SMLG observing thicker snow (up to 40 cm at times). Comparison against the thermistor string buoys individually (representing accumulation over level ice vs. ridged ice) shows moderate correlations with C2I (0.66–0.71) over level ice, albeit with C2I still observing lower snow depth overall. SMLG generally features higher snow depths with weak correlation (0.12) over level ice. The buoy deployed on a ridge shows non-comparable snow depths. It is clear from the buoy comparisons, that making a firm conclusion on the accuracy of C2I or SMLG snow depths with a few in situ time series is challenging. To fully examine the capabilities of C2I snow depth retrieval, it will be necessary to compare with near-coincident reference observations distributed over time and space, preferably from airborne or ground-based campaigns with similar instruments/sensors. Winter 2021–2022 sees thicker snow for both ESA-E and LARM, up to 0.25 m over CA, however still with lower pan-Arctic statistics than seen from the SMLG at 25-km segments.

We also investigate bimonthly snow depth distributions of a full pan-Arctic coverage of gridded IS2/CS2 (LaKu) snow depths for the winter season 2020–2021 (Figures 4m–4r) and 2021–2022 (Figures 5j–5l). For 2020–2021, thinner snow depths are observed for PA in the beginning of the season compared to C2I with similar snow depths observed by the end of the season. There is higher variability for gridded snow depths in CA than observed by C2I. The differences in the shapes of the distributions can be related to the difference in data coverage between C2I and LaKu. For instance, the much thicker snow of CA (tail and bimodality of distribution) is not observed in C2I due to limited observations in the area directly north of Ellesmere Island and Greenland. For 2021–2022, the same bimodal distribution is not that distinctive. For 2021–2022, the spaceborne observations (C2I) are more similar to the monthly estimates (LaKu) in terms of averages. The inconsistent and incomplete C2I data coverage across the Arctic also impacts the estimation of the seasonal snow accumulation rates (Figures 6a–6d). Here, the accumulation rates are separated into zones of FYI and MYI (based on AMSR2 ice type classification). Over FYI the C2I snow depths accumulate by ∼0.09 m with similar magnitude and at a similar rate to the SMLG and mW99 estimates. However, the snow depths from AMSR2 are thicker. The AMSR2 estimates also show a consistent snow depth reduction between January and April in 2020–2021. Over MYI, the C2I snow depths are similar to
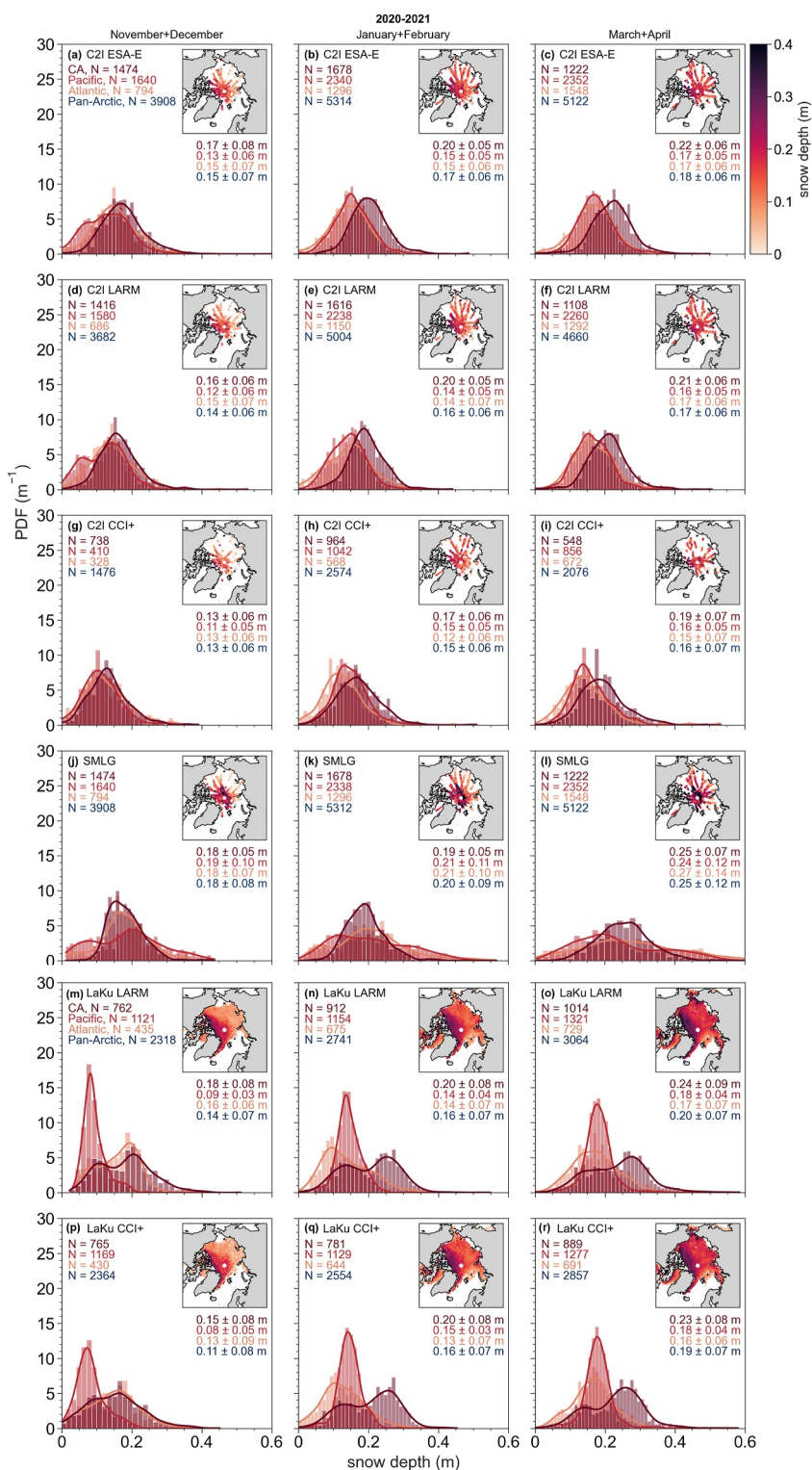
Figure 4. Bimonthly distributions of 25 km orbit-segment snow depth estimates separated by geographical areas (Figure 1): Canadian Arctic (CA), Pacific and Central Arctic (Pacific) and the Atlantic Arctic (Atlantic). Pan-Arctic statistics are provided in dark blue. Number of observations, average snow depth and standard deviation are provided. Pan-Arctic map with C2I tracks locations and corresponding snow depth are shown. (m–r) Bimonthly LaKu gridded snow depth composites.
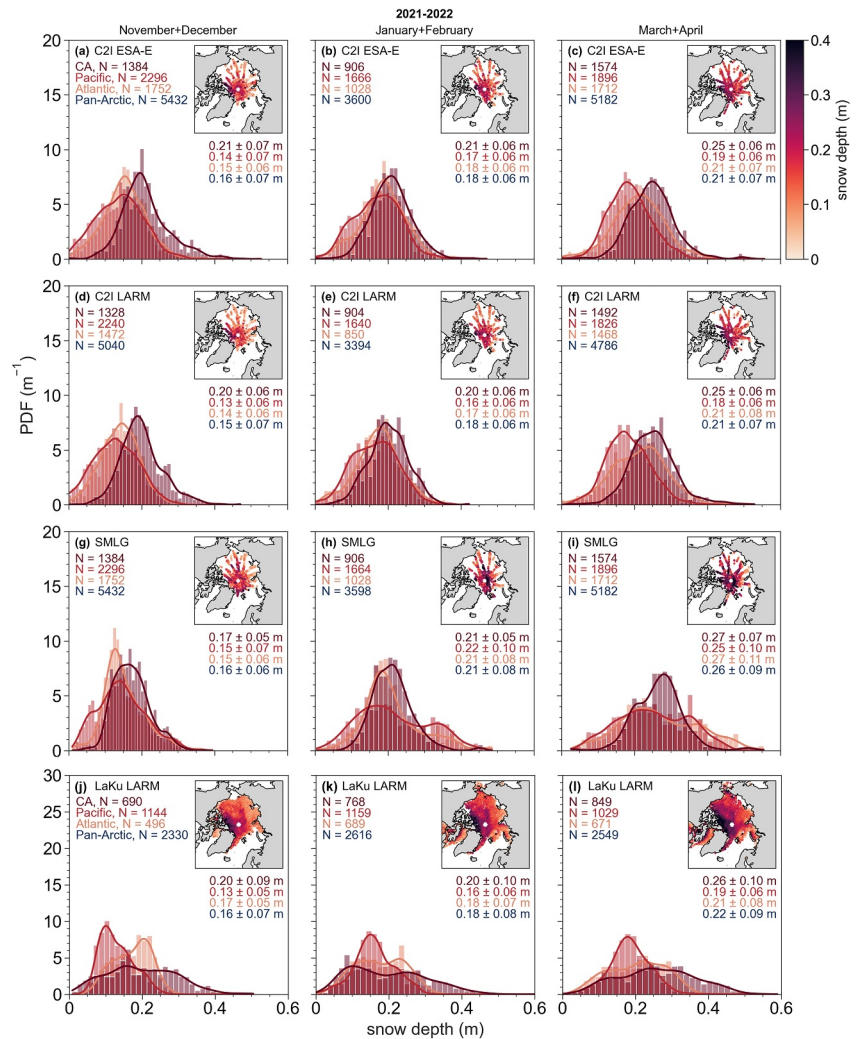
Figure 5. Same as Figure 4 for 2021–2022, but without CCI+ as the data product was unavailable.

SMLG at the beginning of the season but ∼0.10 m thinner by April. The dense region of C2I observations close to the polar hole, as well as the entire CA area, are classified as MYI using AMSR2, where the snow depth accumulation rates show limited accumulation. The accumulation rates of 2021–2022 are more similar across the different products with AMSR2 being constantly a little higher, and SMLG acummulating more for both MYI and FYI by the end of the season.

To investigate the seasonal accumulation in the Central Arctic in more detail, we have studied the average IS2 and CS2 freeboards individually (Figures 6e–6i). Here, we see that IS2 increases significantly with approximately 0.20 m over FYI, and 0.07 m for MYI. CS2 both increases and decreases during the season, reflecting the competition between processes of ice growth (increasing radar freeboard) and snow loading (decreasing free-board). If the radar freeboards remained unchanged and to match SMLG accumulation over MYI, the IS2 laser freeboards need to thicken by 0.14 m rather than 0.07 m over the season. In contrast, if the laser freeboards remained unchanged, to match SMLG over MYI, the CS2 radar freeboards would need to reduce by 0.05 m over the winter rather than increasing by ∼0.02 m. Of course, this assumes CS2 and IS2 accurately record the true snow-ice and air-snow interface elevations, respectively. The relatively low C2I snow depth accumulation rate over MYI may also suggest that over thicker snow and older ice, the CS2 radar signal only penetrates a limited depth into the snow (as proposed by Ricker et al., 2015) as potentially suggested by the along-track observations
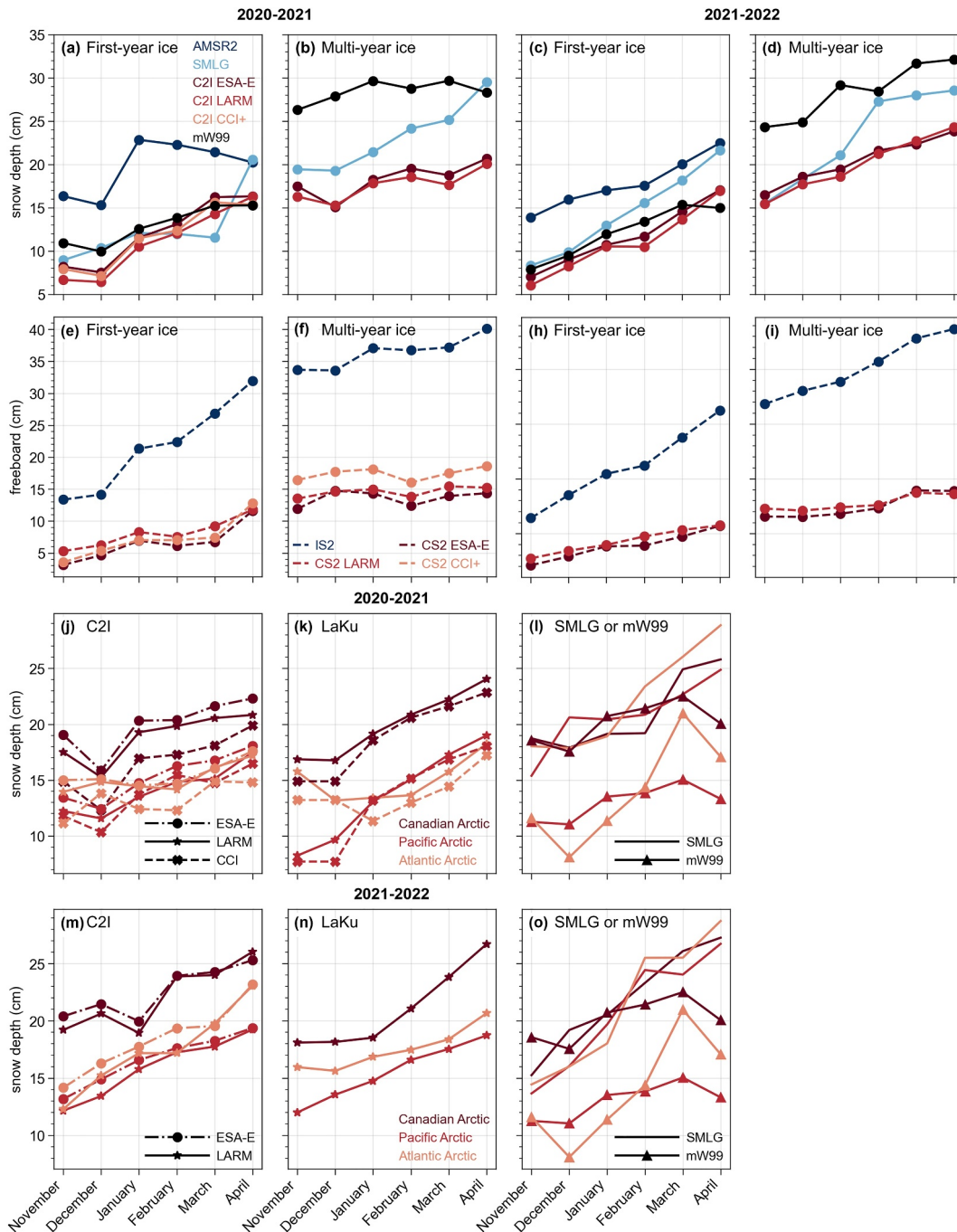
Figure 6. Accumulation rates computed for C2I observations. Note here, that the ice classification is based on availability of AMSR2 data, and the ice mask used for the AMSR2 snow depth product. (a–d) shows C2I snow depth accumulation for both winter seasons, (e–i) shows the laser of radar freeboard accumulation, and (j–o) presents snow depth accumulation rates at 25 km orbit segments (ESA-E, LARM and CCI+)—same as panel (c) but divided by sectors, along with gridded LaKu (here, only LARM and CCI+) product, and SMLG (at C2I 25 km orbit segments resolution) or modified W99 (mW99, re-gridded to LaKu resolution) for the geographical areas of interest.

in Figure 3e. The sensitivity of CS2 radar freeboard observations to short-term fluctuations in height following synoptic weather/snow-depth events has been recently documented (Nab et al., 2023). Such weather events and snow accumulation could cause the increase in the CS2 freeboards and scattering horizon due to limited snow pack penetration and/or reflection within snow pack. The distinction into sectors and comparison with LaKu, shows that C2I is to some extent affected by the inconsistency in data coverage which is evident when investigating accumulation rates (Figures 6j–6o, where accumulation rates are different for C2I and Laku likely due to

the inconsistent data coverage). This is most prevalent for the beginning of the season in PA, where the lowest snow depths are absent in C2I, and with slightly lower snow depths over CA for C2I compared with LaKu. It is noteworthy that PA, for C2I, is more consistent between all three re-trackers, whereas larger discrepancies are observed in the two sectors, CA and AT, where high precipitation rates and greater sea ice deformation occurs. SMLG (Figure 6i) has more than double the accumulation rate over CA, and a significantly higher accumulation rate over PA and AT, when compared to both LaKu and C2I observations. Accumulation pattern of mW99 shows large variations from the other snow depth estimates, which is likely due to the application factor of 0.5 over FYI.

3.3. Random Errors and Systematic Biases: Cross-Over Analysis and Uncertainty Estimation

The differences between XOs (using a maximum of 24 hr delay, however all XOs where within 6 hr) are shown in Figures 7a and 7f, and provides an estimate of random errors. The contribution of the random errors along with difference across re-trackers and maximum absolute systematic bias across re-trackers (Figures 7b–7c and 7g–7h), is used to compute the overall uncertainty. Here, we compute an uncertainty estimate per C2I sample from the local maximum absolute systematic bias per sample (estimates from differences between re-trackers presented in Figures 7b and 7g) and C2I random errors computed from RMSD estimates for all four freeboard estimates. The overall uncertainty ranges (5–95% confidence interval) between 7–16 cm in 2020–2021 and 7–14 cm in 2021–2022, with an average of 11 ± 3 cm for 2020–2021 and 10 ± 2 cm for 2021–2022. One can also investigate uncertainties based on individual re-trackers (and not a combination of all three), where for 2020–2021, CCI+ has the highest uncertainties (but fewest observations). It is important to note, that former dual-frequency snow depth products at grid resolutions of 12.5–25 km have reported overall uncertainties in the order of 6–8 cm (Lawrence et al., 2018) and 3–5 cm (Garnier et al., 2021). We expect higher uncertainties for the random error component at C2I resolution as compared to former studies since grid-averaging minimizes the random noise. We also note that potential systematic biases of IS2 have not been taken into account, and therefore this uncertainty estimate should be considered a minimum estimate. An optimal interpolation strategies, for example, see Landy et al. (2020) could potentially be used to reduce the systematic freeboard uncertainties, benefiting from observations of the sea level anomaly at leads on all aligned tracks to compute the component CS2 and IS2 freeboards.

When considering systematic biases of IS2, its worthy to consider the impact on precision there is from including all six beams in the binning of IS2 observations. While studies have investigated the overall precision of IS2's weak and strong beams in the Arctic (Ricker et al., 2023) along with inter-beam discrepancies (Bagnardi et al., 2021), it is not clear exactly what the impact is on derived freeboards over sea ice. The weak beams are ∼1/4th of the strong beams, and thus we expect lower precision and longer segment-lengths of ATL10 when using weak beams (Bagnardi et al., 2021 also noted that preliminary studies of the IS2 Project Science Office have identified range biases across the beams of centimetre-levels), as the study by Bagnardi et al. (2021) identified an overall a small inter-beam bias on sea surface height anomalies over the Arctic Ocean between the strong beams of beam-pair 1 (GT1R) and beam-pair 3 or 5 (GT3R/GT5R) of ∼3 cm. One could consider using only the strong beams (and potentially only one beam) to limit potential impact on precision, however as we have shown (Figure S1 in Supporting Information S1), limited data was available when generating C2I tracks when considering small search radii (by excluding beam-pairs far away), and when using only strong beams (not shown). Figure 1 shows the separation into strong/weak beams for each season. Here, we see that the majority of 2020–2021 observations originate from the strong beams (GT1-3R, 52.9%), as opposed to 2021–2022 where only 36.0% of observations originated from strong beams. While the average distance between IS2 observations and CS2 observations were similar, this likely also explains the drop in observations between the years.

3.4. Interpretation of C2I Over Sea Ice and Changes Within the Snow and Ice Pack

To compute snow depth from the difference between freeboards, the change in speed once the radar pulse travels through the snow pack must be taken into account. This is achieved through η_s, which relies on the bulk density of snow (ρ_s). For this study, we have used a constant value of 300 kg/m^3 as often used in satellite altimetry studies (e.g., Tonboe et al., 2010; Zwally et al., 2008). Increasing ρ_s will result in an increase in η_s, which in turn will decrease the snow depth observations when following Equation 1. Investigating the impact of using different density ranges (see Figure S6 and Text S8 in Supporting Information S1), by utilizing the densities of Mallett et al. (2020) which are also commonly used for altimetry studies (e.g., Garnier et al., 2021), we observe differences ranging from −2 to 6 mm. While the varying (ρ_s) does not have a large impact on the snow depth estimates of dual-
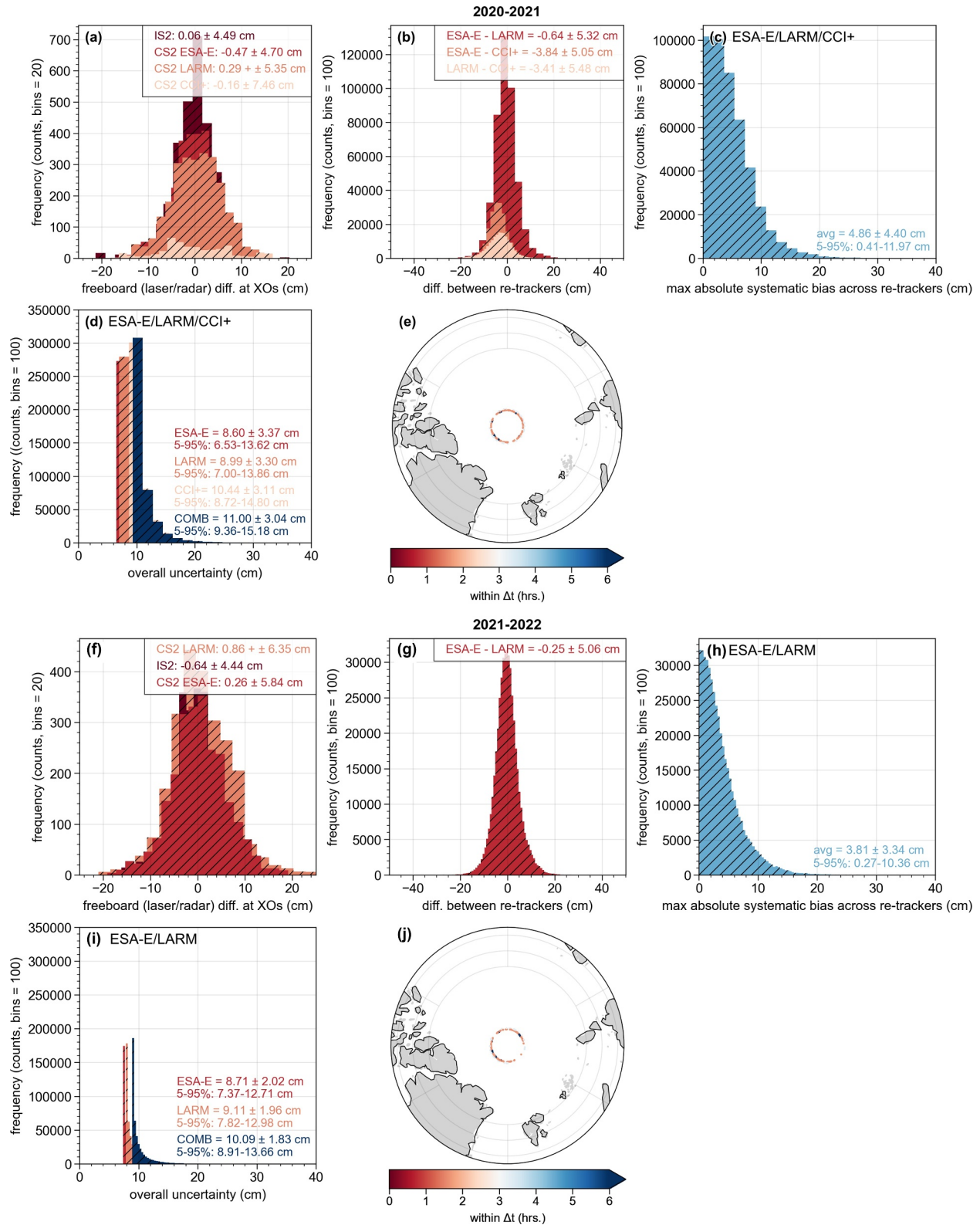
Figure 7. Identified cross-overs (XOs), and distributions of random errors, systematic bias and uncertainty. (a) differences (diff.) between XOs pairs for all parameters of interest, (b) height diff. for freeboard between re-trackers, (c) maximum absolute systematic bias pr. C2I point, (d) uncertainty of C2I snow depths, (e) identified XO within search radius of 3.5 km and 24 hr, for winter season 2021–2022. Panels (f–j) same as panels (a–e) for winter season 2021–2022.

frequency altimetry (density uncertainty of approximately 0.01 m), it has a larger impact on the conversion from freeboard to sea ice thickness when accounting for the slower wave propagation speed in snow (Mallett et al., 2020).

This methodology of dual-frequency snow depth retrieval relies on the assumption that Ku-band radar waves penetrate through the snow pack and are reflected at the snow-ice interface. It also relies on the assumption that laser freeboards from IS2 (or radar freeboard from Ka-band) accurately represent the height of the mean air-snow interface elevation above sea level. While the assumption for Ku-band penetration in snow has been supported by laboratory experiments (Beaven et al., 1995), several studies have disputed that the assumption is valid for all winter and spring conditions of the Arctic sea ice pack (King et al., 2018; Nab et al., 2023; Stroeve et al., 2022; Tonboe et al., 2021; Willatt et al., 2010, 2011). Due to the high local variability of snow processes and conditions, caused by changes in atmospheric forcing, snow grain metamorphism, new precipitation, and snow redistribution in dunes and drifts, laboratory conditions of simple homogeneous snow rarely apply for the Arctic snow pack throughout a winter season (Willatt et al., 2023). Various events like rain-on-snow (Stroeve et al., 2022), flooding of snow packs and refreezing (snow-ice formation), changes in snow salinity (Nandan et al., 2017), brine wicking (Nandan et al., 2020; Rösel et al., 2021), and more, can change the geophysical properties of the snow pack and the principal back scattering horizon that is likely to be encountered by the propagating radar signal (Stroeve et al., 2022; Tonboe et al., 2021). The study of Nab et al. (2023) presented some of the first results of synoptic variability in spaceborne altimeter-derived radar freeboards, where they suggested that in the period immediately after a snowfall, radar pulses are not scattered from the snow-ice interface. Furthermore, De Rijke-Thomas et al. (2023) showed that the radar-scale roughness and slope distributions of the air-snow and snow-ice interfaces strongly impact Ku-band radar scattering from a nadir-looking airborne sensor, suggesting that smoother snow-ice interfaces characteristic of FYI can be more likely to accurately detect the snow-ice interface elevation. An interesting future research question would therefore be to test the derived snow depth distributions for C2I samples acquired after new snowfall versus in stable conditions. Lawrence et al. (2018) used airborne observations to calibrate Ku-band CS2 and ENVISAT radar freeboards, reducing them with respect to the raw data and arguing this reduction was necessary partly due to incomplete penetration of the radar into the snow. If the radar penetration needs to be corrected, it would result in an increase in the C2I snow depths presented here and a potentially closer match to SMLG later in the winter.

Furthermore, there are uncertainties related to the laser freeboards derived from IS2. As examples, including dark and/or specular leads in the surface classification changes the basin-scale mean laser freeboard by 0.00–0.04 m (Kwok et al., 2021) and IS2 misses a portion of ridges and rougher topography over sea ice which is otherwise captured by airborne laser scanners (Ricker et al., 2023). Thus, there is a chance that systematic uncertainty in IS2 freeboard also causes the winter C2I rates of snow accumulation to be underestimated. While several studies are currently investigating ground-based Ku- and Ka-band observations (Stroeve et al., 2020, 2022; Willatt et al., 2023), few studies have investigated airborne dual-frequency altimetry observations over sea ice. The C2I Arctic/Antarctic under-flight performed in July/December 2022 presents an opportunity to investigate this further and interpret radar and laser freeboards obtained at satellite scales, albeit in summer Arctic/Antarctic sea ice conditions which may present additional challenges. However, it will allow for further investigation of radar waveforms and observations obtained at higher resolution, which can be compared with satellites and the possibility of bridging between spatial scales can be further evaluated.

When binning observations acquired over sea ice to a similar spatial resolution, although acquired in different ways (re-tracking of waveform compared to photon-aggregated-elevation estimates), it is important to consider the expected covariance of the observations and the ultimate objective of the study. Currently, we have compared smoothed C2I estimates (7 km window) on orbit-segments of 25 km, but CRISTAL requirements state snow depth estimates must be determined with low uncertainty at segments of less than or equal to 25 km. So, whilst it is unrealistic to use the CS2 raw sampling rate for snow depth retrieval due to along-track noise, we should consider at what sampling rate the snow depth variability starts to be realistic. This requires independent reference observations of snow depth. A comparison with airborne under-flights will allow for further investigation of the length scales at which snow depth can be retrieved from space with reasonable accuracy. Here, airborne snow depth observations using a-snow-radar (2–18 GHz or 2–8 GHz) have been investigated and validated against near-coincident in situ observations for Arctic sea ice (e.g., Farrell et al., 2012; Jutila et al., 2022; Kwok et al., 2017; Panzer et al., 2013; Rösel et al., 2021) during periods with large sea ice extent (March-April during campaigns conducted in 2009–2018). While airborne snow depth over Antarctic sea ice have only been investigated (Fons & Kurtz, 2019; Kwok & Maksym, 2014) during October-November in 2010–2012, but not validated

against in situ observations. Airborne snow depth retrievals of Ka/Ku/La combinations (and compared with snow-radar retrievals) still needs further development and investigation in both hemispheres as Ka/Ku/La-combinations have primarily been used for comparison with satellite observations rather than being validated themselves. This is crucial, especially for the summer season where currently two CRYO2ICE under-flights (Arctic and Antarctic) have been conducted, and where the Antarctic campaign carried the unique combination of frequency-bands and instruments (La/Ku/Ka/S/C-band) simultaneously. Since Antarctic sea ice primarily consists of FYI with a thicker snow cover compared to the Arctic due to heavy precipitation, the thick snow pack can cause floes to depress below the water surface, resulting in negative freeboards or flooding of the floe and snow pack. This can lead to re-freezing and snow-ice formation which are snow-ice interactions that make it difficult to say from which surface the radar is scattered from. Simultaneously, a thick snow cover also limits the penetration of the Ku-band radar, which would result in reduced snow depths.

3.5. C2I as a Proxy for CRISTAL—Differences Between Laser and Ka-Band Elevations

If we were to directly relate C2I to CRISTAL, we would have to make the assumption that laser photons and Ka-band radar waves scatters at the same height. However, studies have shown that Ka-band primarily backscatters from midway and upwards in the snow pack (Armitage & Ridout, 2015), and Lawrence et al. (2018) showed a need to calibrate AltiKa (Ka-band) heights upwards relative to airborne laser observations. In addition, Garnier et al. (2021) showed that for airborne observations, snow depths derived from Ka/Ku-band were consistently lower than snow depths derived from La/Ku-band. As such, there is a dissimilarity between laser and Ka-band that must be addressed if we were to consider C2I as a proxy for CRISTAL. Our results here show that near-coincident 7-km segment La/Ku-band snow depths produce total uncertainty estimates of >6 cm with averages around 10–11 cm, which is higher than the 5 cm at 25-km scale requirement for CRISTAL snow depths (Kern et al., 2020). CRISTAL snow depths should be more precise than C2I with coinciding sensor footprints between Ku- and Ka-band radars observing the same targets; however, they may be less precise owing to the outstanding uncertainties of Ka-band and Ku-band scattering in snow and from snow-ice and air-snow interfaces. The height of maximum scattering intensity at Ka-band will be further investigated once CRISTAL (and CRISTALAir, the airborne simulator of CRISTAL) is launched. Here, it will be crucial to have coincident airborne observations at various frequencies (laser, Ka-band, and Ku-band) to investigate how changes in snow and ice conditions impact the retrieved freeboards (as discussed in De Rijke-Thomas et al., 2023). The airborne observations of the C2I Antarctic under-flight will provide some of the first means to fully investigate this along the orbits where dual-frequency altimetry has been used to estimate snow depth, as the Cryo2IceEx/NERC DEFIANT Antarctic under-flight flew with both Ka-band, Ku-band, laser and a snow radar along a C2I orbit.

Data Availability Statement

Data used and produced in this study is available from https://data.dtu.dk/articles/dataset/CRYO2ICE_radar_laser_freeboards_snow_depth_on_sea_ice_and_comparison_against_auxiliary_data_during_winter_season_2020-2021/21369129 (last access: 2024/01/25) at Data DTU via https://doi.org/10.11583/DTU.21369129 (Fredensborg Hansen et al., 2024), and the code is available on https://github.com/reneefredensborg/CRYO2ICE-Arctic-freeboards-and-snow-depth-2020-2022 (last access: 2024/01/25). CS2 Baseline-E L2 products along with IS2 ATL10 products were retrieved through www.cryo2ice.org (last access: 2022/03/02, now known as www.cs2eo.org, last access: 2024/01/22), where the code for retrieval (provided by the tool) of the data is available at the GitHub repository. Additional Baseline-E (non-C2I tracks) were downloaded from https://science-pds.cryosat.esa.int/ (last access: 2021/01/22). CS2 LARM radar freeboard product was provided by JCL, presented in (Landy et al., 2020), along with gridded LARM and mW99 observations. CS2 CCI+ radar freeboards are available from https://ftp.awi.de/sea_ice/projects/cci/crdp/v3p0-rc1/cryosat2/nh/l2p_trajectory/ (last access: 2022/10/25) (see more in e.g., Hendricks et al., 2023; Rinne & Hendricks, 2023), and the gridded products are available from https://ftp.awi.de/sea_ice/projects/cci/crdp/v3p0-rc1/cryosat2/nh/l3c_grid/ (last access: 2023/05/24). ATL20 was retrieved from NasaEarthData (Petty et al., 2021) (last access: 2024/01/24). Passive-microwave product is available at the National Snow and Ice Data Center (NSIDC) as AMSR-E/AMSR2 Unified L3 Daily 12.5 km Brightness Temperatures, Sea Ice Concentration, Motion & Snow Depth Polar Grids, Version 1 (AU_SI12) (Meier et al., 2018), last access: 2022/10/12. SMLG product is available at NSIDC as Lagrangian Snow Distributions for Sea-Ice Applications, Version 1 (NSIDC-0758) (Liston et al., 2021), last access: 2022/10/

12 with the newest version (extended to cover period of study) provided by IM. Autonomous sea ice measurements (snow depth buoys from AWI) from 2020/10/01 to 2021/04/30 were obtained from https://www.meer-eisportal.de (Grant REKLIM-2013-04) with https://doi.org/10.1594/PANGAEA.875638 (Nicolaus et al., 2021). SIMBA buoy snow depths were provided by Ruibo Lei. Sea ice drift observations were retrieved from OSI SAF Medium Resolution Sea Ice Drift, OSI-407-a. EUMETSAT Ocean and Sea Ice Satellite Application Facility (EUMETSAT, 2024) (last access: 2024/01/20).

References

Alford, J., Ewart, M., Bizon, J., Easthope, R., Gourmelen, N., Parrinello, T., et al. (2021). *CRYO2ICE coincident data explorer.* Version 1. European Space Agency. Retrieved from http://cryo2ice.org

Armitage, T. W. K., & Davidson, M. W. J. (2014). Using the interferometric capabilities of the ESA CryoSat-2 mission to improve the accuracy of sea ice freeboard retrievals. *IEEE Transactions on Geoscience and Remote Sensing*, *52*(1), 529–536. https://doi.org/10.1109/TGRS.2013.2242082

Armitage, T. W. K., & Ridout, A. L. (2015). Arctic sea ice freeboard from AltiKa and comparison with CryoSat-2 and Operation Icebridge. *Geophysical Research Letters*, *42*(16), 6724–6731. https://doi.org/10.1002/2015GL064823

Bagnardi, M., Kurtz, N. T., Petty, A. A., & Kwok, R. (2021). Sea surface height anomalies of the Arctic Ocean from ICESat-2: A first examination and comparisons with CryoSat-2. *Geophysical Research Letters*, *48*(14), e2021GL093155. https://doi.org/10.1029/2021GL093155

Beaven, S. G., Lockhart, G. L., Gogineni, S. P., Hossetnmostafa, A. R., Jezek, K., Gow, A. J., et al. (1995). Laboratory measurements of radar backscatter from bare and snow-covered saline ice sheets. *International Journal of Remote Sensing*, *16*(5), 851–876. https://doi.org/10.1080/01431169508954448

De Rijke-Thomas, C., Landy, J. C., Mallett, R., Willatt, R. C., Tsamados, M., & King, J. (2023). Airborne investigation of quasi-specular Ku-band radar scattering for satellite altimetry over snow-covered Arctic sea ice. *IEEE Transactions on Geoscience and Remote Sensing*, *61*, 1–19. https://doi.org/10.1109/TGRS.2023.3318263

EUMETSAT. (2024). OSI SAF Medium Resolution Sea Ice Drift, OSI-407-a [Dataset]. *EUMETSAT Ocean and Sea Ice Satellite Application Facility*. Retrieved from https://osi-saf.eumetsat.int/products/osi-407-a

European Space Agency. (2019). *CryoSat-2 product handbook Baseline E 1.0 - draft B*. European Space Agency. Retrieved from https://earth.esa.int/eogateway/documents/20142/0/CryoSat-Product-Handbook-Baseline-E-draft.pdf/fc311af8-b926-cf59-5e3a-6b81942e262f(C2-LI-ACS-ESL-5319

Farrell, S. L., Kurtz, N., Connor, L. N., Elder, B. C., Leuschen, C., Markus, T., et al. (2012). A first assessment of Icebridge snow and ice thickness data over Arctic sea ice. *IEEE Transactions on Geoscience and Remote Sensing*, *50*(6), 2098–2111. https://doi.org/10.1109/TGRS.2011.2170843

Fons, S. W., & Kurtz, N. T. (2019). Retrieval of snow freeboard of Antarctic sea ice using waveform fitting of CryoSat-2 returns. *The Cryosphere*, *13*(3), 861–878. https://doi.org/10.5194/tc-13-861-2019

Fredensborg Hansen, R. M., Rinne, E., Farrell, S. L., & Skourup, H. (2021). Estimation of degree of sea ice ridging in the Bay of Bothnia based on geolocated photon heights from ICESat-2. *The Cryosphere*, *15*(6), 2511–2529. https://doi.org/10.5194/tc-15-2511-2021

Fredensborg Hansen, R. M., Skourup, H., Rinne, E., Høyland, K. V., Landy, J., Merkouriadi, I., & Forsberg, R. (2024). CRYO2ICE radar/laser freeboards, snow depth on sea ice and comparison against auxiliary data during winter seasons 2020–2022 [Dataset]. https://data.dtu.dk/articles/dataset/CRYO2ICE_radar_laser_freeboards_snow_depth_on_sea_ice_and_comparison_against_auxiliary_data_during_winter_season_2020-2021/21369129

Garnier, F., Fleury, S., Garric, G., Bouffard, J., Tsamados, M., Laforge, A., et al. (2021). Advances in altimetric snow depth estimates using bi-frequency SARAL and CryoSat-2 Ka–Ku measurements. *The Cryosphere*, *15*(12), 5483–5512. https://doi.org/10.5194/tc-15-5483-2021

Giles, K., Laxon, S., Wingham, D., Wallis, D., Krabill, W., Leuschen, C., et al. (2007). Combined airborne laser and radar altimeter measurements over the Fram Strait in May 2002. *Remote Sensing of Environment*, *111*(2), 182–194. (Remote Sensing of the Cryosphere Special Issue). https://doi.org/10.1016/j.rse.2007.02.037

Grosfeld, K., Treffeisen, R., Asseng, J., Bartsch, A., Bräuer, B., Fritzsch, B., et al. (2016). Online sea-ice knowledge and data platform <www.meereisportal.de>. *Polarforschung*, *85*(2), 143–155. https://doi.org/10.2312/polfor.2016.011

Guerreiro, K., Fleury, S., Zakharova, E., Rémy, F., & Kouraev, A. (2016). Potential for estimation of snow depth on Arctic sea ice from CryoSat-2 and SARAL/AltiKa missions. *Remote Sensing of Environment*, *186*, 339–349. https://doi.org/10.1016/j.rse.2016.07.013

Hendricks, S., Paul, S., & Rinne, E. (2023). ESA Sea Ice Climate Change Initiative (Sea_Ice_CCI): Northern hemisphere sea ice thickness from CryoSat-2 on the satellite swath (L2P), v2.0 [Dataset]. *Reference D4.2, Phase 1.* https://doi.org/10.5285/5b6033bfb7f241e89132a83fdc3d5364

Itkin, P., Hendricks, S., Webster, M., von Albedyll, L., Arndt, S., Divine, D., et al. (2023). Sea ice and snow characteristics from year-long transects at the MOSAiC central observatory. *Elementa: Science of the Anthropocene*, *11*(1). https://doi.org/10.1525/elementa.2022.00048

Jackson, K., Wilkinson, J., Maksym, T., Meldrum, D., Beckers, J., Haas, C., & Mackenzie, D. (2013). A novel and low-cost sea ice mass balance buoy. *Journal of Atmospheric and Oceanic Technology*, *30*(11), 2676–2688. https://doi.org/10.1175/JTECH-D-13-00058.1

Jutila, A., King, J., Paden, J., Ricker, R., Hendricks, S., Polashenski, C., et al. (2022). High-resolution snow depth on Arctic sea ice from low-altitude airborne microwave radar data. *IEEE Transactions on Geoscience and Remote Sensing*, *60*, 1–16. https://doi.org/10.1109/TGRS.2021.3063756

Kacimi, S., & Kwok, R. (2020). The Antarctic sea ice cover from ICESat-2 and CryoSat-2: Freeboard, snow depth, and ice thickness. *The Cryosphere*, *14*(12), 4453–4474. https://doi.org/10.5194/tc-14-4453-2020

Kacimi, S., & Kwok, R. (2022). Arctic snow depth, ice thickness, and volume from ICESat-2 and CryoSat-2: 2018–2021. *Geophysical Research Letters*, *49*(5), e2021GL097448. https://doi.org/10.1029/2021GL097448

Kern, M., Cullen, R., Berruti, B., Bouffard, J., Casal, T., Drinkwater, M. R., et al. (2020). The Copernicus polar ice and snow topography altimeter (CRISTAL) high-priority candidate mission. *The Cryosphere*, *14*(7), 2235–2251. https://doi.org/10.5194/tc-14-2235-2020

King, J., Howell, S., Brady, M., Toose, P., Derksen, C., Haas, C., & Beckers, J. (2020). Local-scale variability of snow density on Arctic sea ice. *The Cryosphere*, *14*(12), 4323–4339. https://doi.org/10.5194/tc-14-4323-2020

King, J., Skourup, H., Hvidegaard, S. M., Rösel, A., Gerland, S., Spreen, G., et al. (2018). Comparison of freeboard retrieval and ice thickness calculation from ALS, ASIRAS, and CryoSat-2 in the Norwegian Arctic to field measurements made during the N-ICE2015 expedition. *Journal of Geophysical Research: Oceans*, *123*(2), 1123–1141. https://doi.org/10.1002/2017JC013233

Kurtz, N. T., & Farrell, S. L. (2011). Large-scale surveys of snow depth on arctic sea ice from Operation Icebridge. *Geophysical Research Letters*, *38*(20). https://doi.org/10.1029/2011GL049216

Kwok, R., Kacimi, S., Webster, M., Kurtz, N., & Petty, A. (2020). Arctic snow depth and sea ice thickness from ICESat-2 and CryoSat-2 freeboards: A first examination. *Journal of Geophysical Research: Oceans*, *125*(3), e2019JC016008. https://doi.org/10.1029/2019JC016008

Kwok, R., Kurtz, N. T., Brucker, L., Ivanoff, A., Newman, T., Farrell, S. L., et al. (2017). Intercomparison of snow depth retrievals over Arctic sea ice from radar data acquired by Operation Icebridge. *The Cryosphere*, *11*(6), 2571–2593. https://doi.org/10.5194/tc-11-2571-2017

Kwok, R., & Maksym, T. (2014). Snow depth of the Weddell and Bellingshausen sea ice covers from Icebridge surveys in 2010 and 2011: An examination. *Journal of Geophysical Research: Oceans*, *119*(7), 4141–4167. https://doi.org/10.1002/2014JC009943

Kwok, R., Petty, A., Bagnardi, M., Wimert, J. T., Cunningham, G. F., Hancock, D. W., & Nathan Kurtz, A. I. (2022). Ice, Cloud, and land Elevation Satellite (ICESat-2) project: Algorithm Theoretical Basis Document (ATBD) for sea ice products (ATL07/ATL10/ATL20/ATL21) release 005. Retrieved from https://nsidc.org/sites/default/files/icesat2_atl07_atl10_atl20_atl21_atbd_r005_1.pdf

Kwok, R., Petty, A. A., Bagnardi, M., Kurtz, N. T., Cunningham, G. F., Ivanoff, A., & Kacimi, S. (2021). Refining the sea surface identification approach for determining freeboards in the ICESat-2 sea ice products. *The Cryosphere*, *15*(2), 821–833. https://doi.org/10.5194/tc-15-821-2021

Landy, J. C., Bouffard, J., Wilson, C., Rynders, S., Aksenov, Y., & Tsamados, M. (2021). Improved Arctic sea ice freeboard retrieval from satellite altimetry using optimized sea surface decorrelation scales. *Journal of Geophysical Research: Oceans*, *126*(12), e2021JC017466. https://doi.org/10.1029/2021JC017466

Landy, J. C., Petty, A. A., Tsamados, M., & Stroeve, J. C. (2020). Sea ice roughness overlooked as a key source of uncertainty in CryoSat-2 ice freeboard retrievals. *Journal of Geophysical Research: Oceans*, *125*(5), e2019JC015820. https://doi.org/10.1029/2019JC015820

Landy, J. C., Tsamados, M., & Scharien, R. K. (2019). A facet-based numerical model for simulating SAR altimeter echoes from heterogeneous sea ice surfaces. *IEEE Transactions on Geoscience and Remote Sensing*, *57*(7), 4164–4180. https://doi.org/10.1109/TGRS.2018.2889763

Launiainen, J., & Cheng, B. (1998). Modelling of ice thermodynamics in natural water bodies. *Cold Regions Science and Technology*, *27*(3), 153–178. https://doi.org/10.1016/S0165-232X(98)00009-3

Lawrence, I. R., Tsamados, M. C., Stroeve, J. C., Armitage, T. W. K., & Ridout, A. L. (2018). Estimating snow depth over Arctic sea ice from calibrated dual-frequency radar freeboards. *The Cryosphere*, *12*(11), 3551–3564. https://doi.org/10.5194/tc-12-3551-2018

Lei, R., Cheng, B., Hoppmann, M., & Zuo, G. (2021). Snow depth and sea ice thickness derived from the measurements of SIMBA buoys deployed in the Arctic Ocean during the Legs 1a, 1, and 3 of the MOSAiC campaign in 2019-2020 [Dataset]. *PANGAEA*. https://doi.org/10.1594/PANGAEA.938244

Leppäranta, M. (1983). A growth model for black ice, snow ice and snow thickness in subarctic basins. *Hydrology Research*, *14*(2), 59–70. https://doi.org/10.2166/nh.1983.0006

Liao, Z., Cheng, B., Zhao, J., Vihma, T., Jackson, K., Yang, Q., et al. (2019). Snow depth and ice thickness derived from SIMBA ice mass balance buoy data using an automated algorithm. *International Journal of Digital Earth*, *12*(8), 962–979. https://doi.org/10.1080/17538947.2018.1545877

Liston, G. E., Itkin, P., Stroeve, J., Tschudi, M., Stewart, J. S., Pedersen, S. H., et al. (2020). A Lagrangian snow-evolution system for sea-ice applications (SnowModel-LG): Part I—Model description. *Journal of Geophysical Research: Oceans*, *125*(10), e2019JC015913. https://doi.org/10.1029/2019JC015913

Liston, G. E., Polashenski, C., Rösel, A., Itkin, P., King, J., Merkouriadi, I., & Haapala, J. (2018). A distributed snow-evolution model for sea-ice applications (SnowModel). *Journal of Geophysical Research: Oceans*, *123*(5), 3786–3810. https://doi.org/10.1002/2017JC013706

Liston, G. E., Stroeve, J., & Itkin, P. (2021). *Lagrangian snow distributions for sea-ice applications, version 1*. NASA National Snow and Ice Data Center Distributed Active Archive Center. https://doi.org/10.5067/27A0P5M6LZBI

Magruder, L. A., Brunt, K. M., & Alonzo, M. (2020). Early ICESat-2 on-orbit geolocation validation using ground-based corner cube retro-reflectors. *Remote Sensing*, *12*(21), 3653. https://doi.org/10.3390/rs12213653

Mallett, R. D. C., Lawrence, I. R., Stroeve, J. C., Landy, J. C., & Tsamados, M. (2020). Brief communication: Conventional assumptions involving the speed of radar waves in snow introduce systematic underestimates to sea ice thickness and seasonal growth rate estimates. *The Cryosphere*, *14*(1), 251–260. https://doi.org/10.5194/tc-14-251-2020

Markus, T., & Cavalieri, D. (2000). An enhancement of the NASA Team sea ice algorithm. *IEEE Transactions on Geoscience and Remote Sensing*, *38*(3), 1387–1398. https://doi.org/10.1109/36.843033

Markus, T., & Cavalieri, D. J. (1998). Snow depth distribution over sea ice in the Southern Ocean from satellite passive microwave data. In M. O. Jeffries (Ed.), *Antarctic sea ice: Physical processes, interactions and variability, Antarct. res. ser* (Vol. 74, pp. 19–39). AGU. https://doi.org/10.1029/ar074p0019

Markus, T., & Cavalieri, D. J. (2009). The AMSR-E NT2 sea ice concentration algorithm: Its basis and implementation. *Journal of the Remote Sensing Society of Japan*, *29*(1), 216–225. https://doi.org/10.11440/rssj.29.216

Markus, T., Neumann, T., Martino, A., Abdalati, W., Brunt, K., Csatho, B., et al. (2017). The Ice, Cloud, and Land Elevation Satellite-2 (ICESat-2): Science requirements, concept, and implementation. *Remote Sensing of Environment*, *190*, 260–273. https://doi.org/10.1016/j.rse.2016.12.029

Meier, W. N., Markus, T., & Comiso, J. C. (2018). AMSR-E/AMSR2 Unified L3 Daily 12.5 km Brightness Temperatures, Sea ice concentration, Motion & Snow depth polar grids, version 1 [Dataset]. *NASA National Snow and Ice Data Center Distributed Active Archive Center*. https://doi.org/10.5067/RA1MIJOYPK3P

Merkouriadi, I., Liston, G. E., Graham, R. M., & Granskog, M. A. (2020). Quantifying the potential for snow-ice formation in the Arctic Ocean. *Geophysical Research Letters*, *47*(4), e2019GL085020. https://doi.org/10.1029/2019GL085020

Moon, W., Nandan, V., Scharien, R. K., Wilkinson, J., Yackel, J. J., Barrett, A., et al. (2019). Physical length scales of wind-blown snow redistribution and accumulation on relatively smooth Arctic first-year sea ice. *Environmental Research Letters*, *14*(10), 260–273. https://doi.org/10.1088/1748-9326/ab3b8d

Nab, C., Mallett, R., Gregory, W., Landy, J., Lawrence, I., Willatt, R., et al. (2023). Synoptic variability in satellite altimeter-derived radar freeboard of Arctic sea ice. *Geophysical Research Letters*, *50*(2), e2022GL100696. https://doi.org/10.1029/2022GL100696

Nandan, V., Geldsetzer, T., Yackel, J., Mahmud, M., Scharien, R., Howell, S., et al. (2017). Effect of snow salinity on CryoSat-2 Arctic first-year sea ice freeboard measurements. *Geophysical Research Letters*, *44*(20), 10419–10426. https://doi.org/10.1002/2017GL074506

Nandan, V., Scharien, R. K., Geldsetzer, T., Kwok, R., Yackel, J. J., Mahmud, M. S., et al. (2020). Snow property controls on modeled Ku-band altimeter estimates of first-year sea ice thickness: Case studies from the Canadian and Norwegian Arctic. *IEEE Journal of Selected Topics in Applied Earth Observations and Remote Sensing*, *13*, 1082–1096. https://doi.org/10.1109/JSTARS.2020.2966432

Nandan, V., Willatt, R., Mallett, R., Stroeve, J., Geldsetzer, T., Scharien, R., et al. (2023). Wind redistribution of snow impacts the Ka- and Ku-band radar signatures of Arctic sea ice. *The Cryosphere*, *17*(6), 2211–2229. https://doi.org/10.5194/tc-17-2211-2023

Neumann, T. A., Martino, A. J., Markus, T., Bae, S., Bock, M. R., Brenner, A. C., et al. (2019). The Ice, Cloud, and Land Elevation Satellite–2 mission: A global geolocated photon product derived from the advanced topographic laser altimeter system. *Remote Sensing of Environment*, *233*, 111325. https://doi.org/10.1016/j.rse.2019.111325

Nicolaus, M., Hoppmann, M., Arndt, S., Hendricks, S., Katlein, C., Nicolaus, A., et al. (2021). Snow depth and air temperature seasonality on sea ice derived from snow buoy measurements. *Frontiers in Marine Science*, *8*. https://doi.org/10.3389/fmars.2021.655446

Panzer, B., Gomez-Garcia, D., Leuschen, C., Paden, J., Rodriguez-Morales, F., Patel, A., et al. (2013). An ultra-wideband, microwave radar for measuring snow thickness on sea ice and mapping near-surface internal layers in polar firn. *Journal of Glaciology*, *59*(214), 244–254. https://doi.org/10.3189/2013JoG12J128

Perovich, D., Richter-Menge, J., & Polashenksi, C. (2023). Observing and understanding climate change: Monitoring the mass balance, motion, and thickness of Arctic sea ice. Retrieved from http://imb-crrel-dartmouth.org

Petty, A. A., Bagnardi, M., Kurtz, N. T., Tilling, R., Fons, S., Armitage, T., et al. (2021). Assessment of ICESat-2 sea ice surface classification with Sentinel-2 imagery: Implications for freeboard and new estimates of lead and floe geometry. *Earth and Space Science*, *8*(3), e2020EA001491. https://doi.org/10.1029/2020EA001491

Petty, A. A., Kwok, R., Bagnardi, M., Ivanoff, A., Kurtz, N., Lee, J., et al. (2020). ATLAS/ICESat-2 L3B daily and monthly gridded sea ice freeboard, version 1 [Dataset]. *NASA National Snow and Ice Data Center Distributed Active Archive Center*. https://doi.org/10.5067/ATLAS/ATL20.001

Ricker, R., Fons, S., Jutila, A., Hutter, N., Duncan, K., Farrell, S. L., et al. (2023). Linking scales of sea ice surface topography: Evaluation of ICESat-2 measurements with coincident helicopter laser scanning during mosaic. *The Cryosphere*, *17*(3), 1411–1429. https://doi.org/10.5194/tc-17-1411-2023

Ricker, R., Hendricks, S., Perovich, D. K., Helm, V., & Gerdes, R. (2015). Impact of snow accumulation on CryoSat-2 range retrievals over Arctic sea ice: An observational approach with buoy data. *Geophysical Research Letters*, *42*(11), 4447–4455. https://doi.org/10.1002/2015GL064081

Rinne, E., & Hendricks, S. (2023). CCI+ Sea Ice ECV Sea Ice thickness product user guide (PUG). *Reference D4.2, Phase 1)*. [Data Product Description Document].

Rösel, A., Farrell, S. L., Nandan, V., Richter-Menge, J., Spreen, G., Divine, D. V., et al. (2021). Implications of surface flooding on airborne estimates of snow depth on sea ice. *The Cryosphere*, *15*(6), 2819–2833. https://doi.org/10.5194/tc-15-2819-2021

Rostosky, P., Spreen, G., Farrell, S. L., Frost, T., Heygster, G., & Melsheimer, C. (2018). Snow depth retrieval on Arctic sea ice from passive microwave radiometers—Improvements and extensions to multiyear ice using lower frequencies. *Journal of Geophysical Research: Oceans*, *123*(10), 7120–7138. https://doi.org/10.1029/2018JC014028

Scagliola, M. (2013). CryoSat footprints: Aresys technical note. (Italy: Aresys/ESA. SAR-CRY2-TEN-6331).

Stroeve, J., Nandan, V., Willatt, R., Dadic, R., Rotosky, P., Gallagher, M., et al. (2022). Rain-On-Snow (ROS) understudied in sea ice remote sensing: A multi-sensor analysis of ROS during MOSAiC. *The Cryosphere Discussions*, *2022*, 1–42. https://doi.org/10.5194/tc-2021-383

Stroeve, J., Nandan, V., Willatt, R., Tonboe, R., Hendricks, S., Ricker, R., et al. (2020). Surface-based Ku- and Ka-band polarimetric radar for sea ice studies. *The Cryosphere*, *14*(12), 4405–4426. https://doi.org/10.5194/tc-14-4405-2020

Sturm, M., Holmgren, J., & Perovich, D. K. (2002). Winter snow cover on the sea ice of the Arctic Ocean at the surface heat budget of the Arctic Ocean (SHEBA): Temporal evolution and spatial variability. *Journal of Geophysical Research: Oceans*, *107*(C10), SHE 23-1-SHE 23-17. https://doi.org/10.1029/2000JC000400

Taylor, J. R. (1939). *An introduction to error analysis - The study of uncertainties in physical measurements* (2nd. ed.). University Science Books.

Taylor, J. R. (1997). *An introduction to error analysis - The study of uncertainties in physical measurements* (2nd. ed.). University Science Books.

Tonboe, R. T., Nandan, V., Yackel, J., Kern, S., Toudal Pedersen, L., & Stroeve, J. (2021). Simulated Ka-and Ku-band radar altimeter height and freeboard estimation on snow-covered Arctic sea ice. *The Cryosphere*, *15*(4), 1811–1822. https://doi.org/10.5194/tc-15-1811-2021

Tonboe, R. T., Pedersen, L. T., & Haas, C. (2010). Simulation of the CryoSat-2 satellite radar altimeter sea ice thickness retrieval uncertainty. *Canadian Journal of Remote Sensing*, *36*(1), 55–67. https://doi.org/10.5589/m10-027

Ulaby, F., Moore, R. K., & Fung, A. K. (1986). *Microwave remote sensing: From theory to applications* (Vol. 3). Artech House.

Vivier, F., & Lourenco, A. (2023). Sea ice thickness and ancillary parameters between the North Pole and Fram Strait from the Ice-T buoy. https://doi.org/10.17882/87766

Warren, S. G., Rigor, I. G., Untersteiner, N., Radionov, V. F., Bryazgin, N. N., Aleksandrov, Y. I., & Colony, R. (1999). Snow depth on Arctic sea ice. *Journal of Climate*, *12*(6), 1814–1829. https://doi.org/10.1175/1520-0442(1999)012⟨1814:SDOASI⟩2.0.CO;2

Willatt, R., Giles, K., Laxon, S., Stone-Drake, L., & Worby, A. (2010). Field investigations of Ku-band radar penetration into snow cover on Antarctic sea ice. *IEEE Transactions on Geoscience and Remote Sensing*, *48*(1), 365–372. https://doi.org/10.1109/TGRS.2009.2028237

Willatt, R., Laxon, S., Giles, K., Cullen, R., Haas, C., & Helm, V. (2011). Ku-band radar penetration into snow cover on Arctic sea ice using airborne data. *Annals of Glaciology*, *52*(57), 197–205. https://doi.org/10.3189/172756411795931589

Willatt, R., Stroeve, J. C., Nandan, V., Newman, T., Mallett, R., Hendricks, S., et al. (2023). Retrieval of snow depth on Arctic sea ice from surface-based, polarimetric, dual-frequency radar altimetry. *Geophysical Research Letters*, *50*(20), e2023GL104461. https://doi.org/10.1029/2023GL104461

Zhou, L., Stroeve, J., Xu, S., Petty, A., Tilling, R., Winstrup, M., et al. (2021). Inter-comparison of snow depth over Arctic sea ice from reanalysis reconstructions and satellite retrieval. *The Cryosphere*, *15*(1), 345–367. https://doi.org/10.5194/tc-15-345-2021

Zwally, H. J., Yi, D., Kwok, R., & Zhao, Y. (2008). ICESat measurements of sea ice freeboard and estimates of sea ice thickness in the Weddell Sea. *Journal of Geophysical Research: Oceans*, *113*(C2). https://doi.org/10.1029/2007JC004284